STRESS-FUNCTION VARIATIONAL METHOD FOR STRESS AND PROGRESSIVE CRACKING ANALYSIS OF POLYMER COMPOSITE LAMINATES

A Thesis
Submitted to the Graduate Faculty
of the
North Dakota State University
of Agriculture and Applied Science

By

Md Shariful Islam

In Partial Fulfillment of the Requirements
for the Degree of
MASTER OF SCIENCE

Major Department:
Mechanical Engineering

November 2023

Fargo, North Dakota

North Dakota State University
Graduate School

Title

Stress-Function Variational Method for Stress and Progressive Cracking Analysis of Polymer Composite Laminates

By

Md Shariful Islam

The Supervisory Committee certifies that this ***disquisition*** complies with North Dakota State University's regulations and meets the accepted standards for the degree of

MASTER OF SCIENCE

SUPERVISORY COMMITTEE:

Dr. Xiangfa Wu
Chair

Dr. Xinnan Wang

Dr. Yao Yu

Dr. Oksana Zholobko

Approved:

November 28, 2023
Date

Dr. Chad Ulven
Department Chair

ABSTRACT

Polymer matrix composites (PMCs) are widely used in various industries, including aerospace, vehicles, sports utilities, and civil infrastructures. Understanding the failure process and mechanisms of PMCs subjected to external loads is crucial for their reliability. This study aims to develop a semi-analytic stress-function variational method for accurate prediction of interfacial stresses and progressive cracking in PMC laminates. The method uses a three-layered cross-ply laminate model with periodic transverse ply cracks, introducing two unknown interfacial shear and normal stress functions at each laminate interface. The stress field is expressed in terms of these stress functions, using Euler-Bernoulli beam theory and elasticity. The method also considers transverse deflections of the plies, resulting in accurate predictions of interface stresses. The method can be used for scaling analysis of interfacial stresses and progressive cracking in PMC laminates as validated by finite element analysis (FEA).

ACKNOWLEDGMENTS

I would like to express my heartfelt gratitude to my thesis advisor, Dr. Xiangfa Wu, for his guidance, encouragement, and unwavering support throughout this research. His insightful feedback and constructive criticism have been invaluable in shaping the direction and quality of this work. I also extend my gratitude to the remaining members of my supervisory committee, namely, Dr. Xinnan Wang, Dr. Yao Yu, and Dr. Oksana Zholobko, for their valuable supports and helps.

I am deeply thankful to the faculty members of the Department of Mechanical Engineering at North Dakota State University (NDSU) for their knowledge-sharing and academic mentorship, which has played a pivotal role in broadening my understanding of the subject matter. I extend my sincere appreciations to my family and friends for their unconditional love, encouragements, and patience during this journey. Their belief in my abilities has been an endless source of motivation.

The research of this thesis work is sponsored by the National Center for Manufacturing Sciences/DOD GVSC, ND Corn Utilization Council, and the Department of Mechanical Engineering at NDSU.

TABLE OF CONTENTS

LIST OF TABLES

LIST OF FIGURES

1. INTRODUCTION

Composite materials are made of at least two phases, i.e., the matrix phase and the reinforcing phase, which enable to provide improved material properties, e.g., the mechanical and physical properties, compared to those of the monolithic matrix and reinforcing constituents. The origin and application of composite materials can be traced back over one thousand years ago. The earliest composite materials as recorded in the literature, known as wattle and daub, were employed for constructing walls [1]. Since then, engineers had been using and developing various composite materials for broad applications. In the last five decades, significant research investigations have been made in scientific community to exploit their superior properties, improve their design, manufacturing, and deployment, and to reduce the fabrication costs, especially the development of modern high-performance carbon-fiber reinforced polymer matrix composites (PMCs) for aerospace and aeronautical structures and clay nanoparticle reinforced polymer composites for modern personal cars and other industrial utilities. Modern advanced PMC science and technology exemplify the development of modern materials technology with a wide range of structural applications due to their excellent mechanical performance, lightweight, high specific strength, and stiffness [2,3,10].

Structurally, the reinforcing fibers in PMCs carry much higher specific strengths than their bulk counterparts. The enhanced strength of the reinforcing fibers is attributed to their reduced presence of internal or surface defects compared to conventional bulk materials. The reinforcing fibers within PMCs are integrated into a resin matrix material in order to effectively withstand high loads. Simultaneously, the polymeric matrix also functions to bind the reinforcing fibers together to load transfer from one fiber to the next and to protect fibers against wear and degradation caused by various environmental factors. Due to the low mechanical properties of

the resin (e.g., polymeric matrix), the mechanical properties of a PMC experience a certain degree of reduction compared to those of reinforcing fibers. Nevertheless, PMCs remain significantly superior to the bulk matrix materials. Advanced PMCs further enhance their high unidirectional mechanical properties by utilizing aligned continuous high-performance fibers, to achieve up to 70% fiber volume ratio. Unidirectional fiber-reinforced PMCs exbibit significant anisotropy, with very high strength and modulus along the fiber direction. However, the material also exhibits a low modulus and strength in the direction perpendicular to the fiber direction. In the context of fiber-reinforced PMCs, the issue of in-plane anisotropy can be addressed through the utilization of angle-ply laminated PMCs (as depicted in Figure 1.1). This particular approach involves the arrangement of multiple plies of laminae, each possessing distinct fiber orientations, in order to achieve the necessary in-plane mechanical properties. The resulting laminate physical and mechanical properties can be optimized via tailoring the fiber orientations and layer stacking sequences, which form an important content in PMC design, fabrication, and applications. However, sufficient precaution should be taken in avoiding large stress concentration and resulting delamination at ply interfaces, especially near free edges, stemming from the mismatches of elastic and thermal properties at two neighboring plies [3-5].

While advanced PMCs are frequently characterized with their high specific strength and stiffness as well as reduced weight compared to their monolithic counterparts, their limited ductility and vulnerability to cracks and notches remain notable concerns. To date, researchers have developed various strategies to enhance their interlaminar fracture toughness, including techniques like stitching, Z-pinning, incorporation of whiskers, or utilization of braided composites. These technological advancements have drawn more attention to PMCs as materials, with the primary challenges in processing and predictable capabilities [6-10].

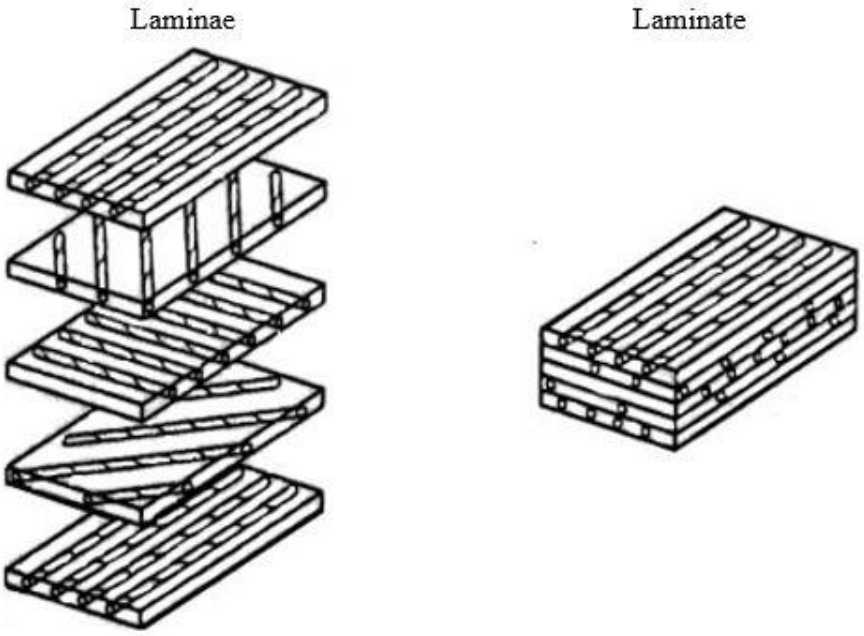

Figure 1.1 Diagrams illustrating the structure of an angle-ply composite laminate (left) and a cross-ply composite laminate (right) [2].

A comprehensive understanding of the failure processes in composite materials under various loading conditions is crucial to establishing a systematic framework for predicting the failure behavior of these materials to ensure their load-carrying capacity, structural reliability and safety. Failure mechanisms must be well-understood in the design and implementation phases to avert the risk of unforeseeable catastrophic structural failure. In contrast to homogeneous materials with their typical failure in term of single-crack propagation, composite materials lack a singular, well-defined failure mechanism. This disagreement is due primarily to the increased anisotropy and constituent inhomogeneity in PMCs. Common failure modes in advanced PMCs encompass transverse matrix cracking, fiber-matrix debonding, fiber breakage, and delamination between laminae [3,10,19].

Amongst all the failure modes, progressive matrix cracking emerges first in the relatively weak and compliant resin of the composite materials, which further lead to other subsequent failure modes due to stress redistribution and concentration that is to be discussed in Chapter 2. In addition, prediction of the interfacial stresses at ply interfaces is critically important, as elevated interfacial stresses can result in delamination at along the ply interfaces. Extensive research has been conducted to develop various rational models to predict the interfacial stresses and matrix cracking in advanced PMCs. So far, quite a few mechanics models of PMCs and joints have been reported in the literature for effective stress analysis of composite laminates and joints, which are often based on oversimplified or even falsified assumptions. For instance, a few such models adopted the assumptions that even fail to satisfy the simple traction-free boundary conditions (BCs) at the PMC or joint edges.

Thus, the goal of this M.S. thesis is to adopt a semi-analytic stress-function variational method for high-efficiency and accurate prediction of the interfacial stresses and progressive matrix cracking in a three-layered cross-ply composite laminate under uniaxial tension. The stress-function variational method, originally developed by Wu and his group [11-16], has been used to predict the interfacial stresses in bonded and adhesively bonded joints. Later, this work was further expanded to predict progressive cracking in hard surface coatings. This highly accurate and effective semi-analytical method enables to provide the precise solutions and incorporate all the BCs that other models fail to address effectively. In addition, the deformation compatibility of the materials is realized in the stress-function variational method via evoking the minimum complementary strain energy theorem.

The present thesis study focuses on a three-layered symmetric cross-ply PMC laminate as a simple laminate model to demonstrate this process. This model introduces two unknown

interfacial shear and normal stress functions at each ply surface. In addition, the planar stress field in each ply is expressed analytically in terms of these interfacial stress functions as follows: the axial normal stresses along the ply direction is assumed to vary linearly according to Euler-Bernoulli beam theory, while the in-planar shear and transverse normal stresses are determined via triggering the stress equilibrium equations of 2D elasticity. The deformation compatibility of the PMC is guaranteed through the minimum complementary strain energy theorem, which results in a set of coupled ordinary differential equations (ODEs) for the interfacial stress functions. This set of ODEs is subsequently solved explicitly using eigenfunctions. The utilization of this method satisfies all the traction boundary conditions, especially the shear-free conditions at edges, which are commonly ignored in conventional analytic methods.

The accuracy and effectiveness of the stress-function variational method for present stress analysis of the three-layered composite laminate are validated by FEM using a commercial software package ANSYS^{TM}. In addition, scaling analysis to examine the dependencies of the interfacial stresses and crack spacing on the laminate geometries and elastic properties changes are made. Consequently. conclusions and suggestions of the present research are made.

2. LITERATURE REVIEW

2.1. Matrix Cracking and Interfacial Stresses

Subjected to external loading, the failure of a PMC laminate is a progressive process of microcrack nucleation, growth, and ultimately catastrophic failure. Common failure modes in advanced PMCs include matrix cracking, fiber-matrix debonding, fiber breakage, and delamination between laminae as shown in Figures 2.1 and 2.2. The actual damage progress in an advanced PMC is contingent upon various factors, including the nature of loading, PMC geometries, and material properties of the PMC constituents, among others. Typically, the damage process is characterized as a stochastic behavior, spreading throughout the composite material. Prior to reaching a catastrophic failure point, damage accumulates gradually and coalesces, ultimately leading to a visible macroscopic fracture. Figure 2.3 illustrates the progressive damage in composite laminates under tensile loading, with five identifiable consecutive damage mechanisms [17]. During the early phase of damage accumulation, there is a noticeable increase in matrix cracking in layers that are oriented perpendicular to the direction of the applied force. In the context of static tensile testing of cross-ply laminates, transverse matrix cracking is detected as early as 0.4-0.5% applied strain, which may vary based on the specific laminate configuration [10].

As stress builds, secondary cracks initiate transversely to the primary intralaminar cracks found in adjacent plies. These secondary cracks are known to induce interlaminar cracks, i.e., interlaminar fracture. In the early stage, these cracks are isolated, and dispersed across the plies. Over time, some of these interlaminar cracks coalesce, forming zone-like strips, which can eventually lead to extensive delamination. This results in a loss of laminate integrity within the

affected regions. In addition, the stresses become highly localized if the load gradually increases, ultimately leading to fiber breakage [3,18].

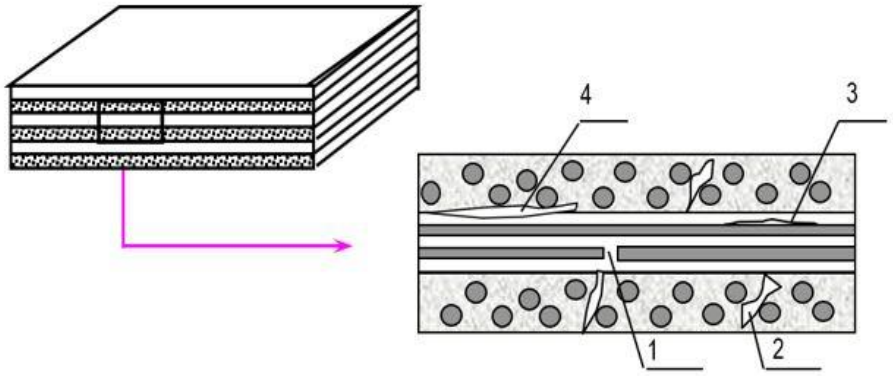

Figure 2.1 The common damage modes of observed in a cross-ply composite material. (1) Fiber breakage; (2) matrix cracking; (3) fiber/matrix debonding; (4) delamination [3].

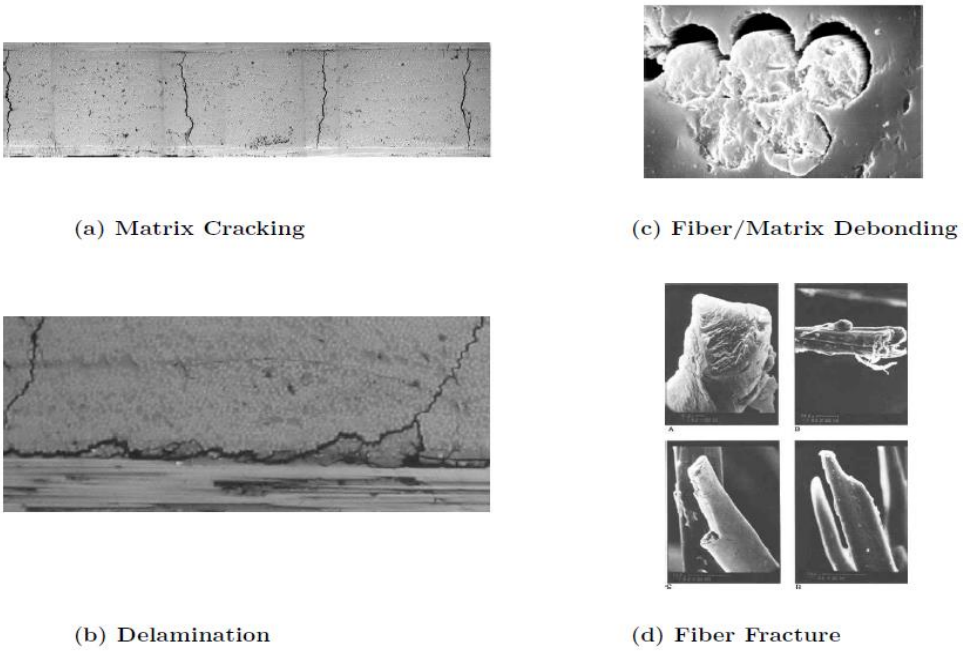

Figure 2.2 Images to show the failure mechanisms of fiber-reinforced composite laminates [10].

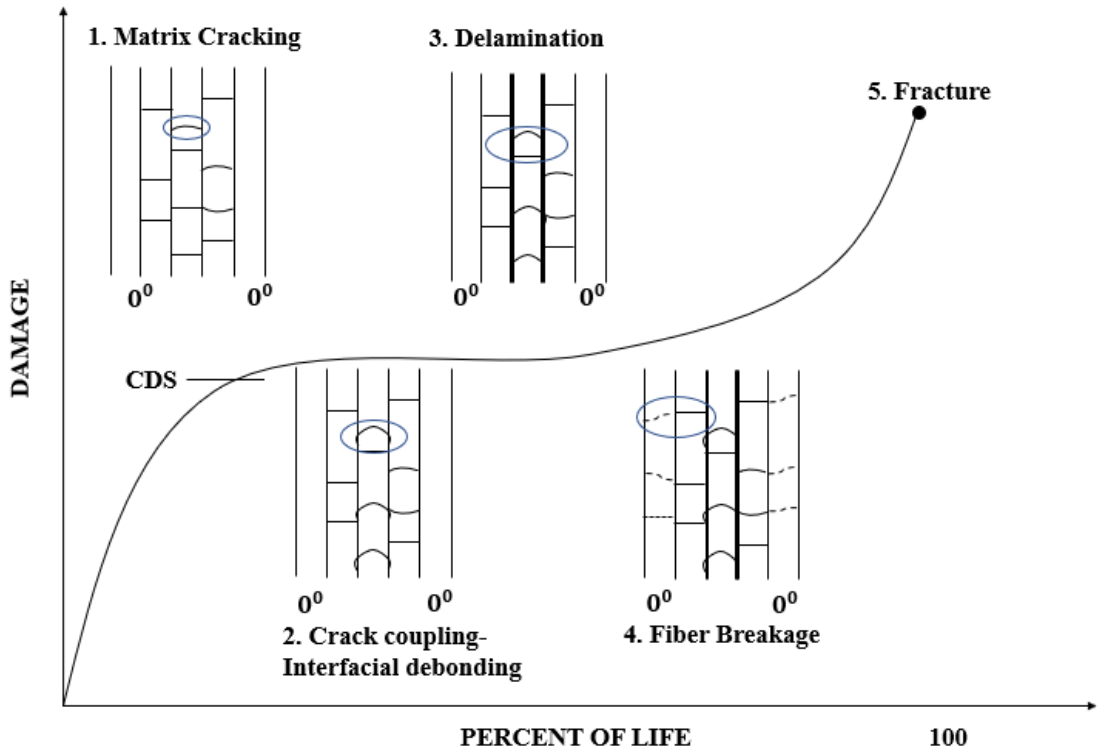

Figure 2.3 Schematic diagram to show the damage development in composite laminates [Reproduced from [19]].

Among various types of damage modes, the first mode frequently observed in composite laminates is matrix cracking. These matrix cracks tend to develop perpendicular to the fiber orientation due to the brittleness and low ultimate tensile strain of the thermosetting resin (e.g., thermosetting epoxy). As the applied load intensifies, the crack density also increases, forming three-dimensional (3D) intersecting cracks spanning through multiple layers in multiple directions. Advanced PMC laminates utilize high-strength and high-modulus fibers embedded within a compliant polymeric resin to form a UD lamina, which delivers the essential load-carrying capacity along the fiber direction. When subjected to tensile loading along the fiber direction, this UD lamina undergoes tensile failure due to fiber rupture. Because the reinforcing fibers are much stiffer than the polymeric matrix, a considerable strain can exert within the

matrix when a ply is subjected to transverse loading. The off-axis plies have a lower failure strain than those aligned with the loading direction. Consequently, a UD lamina exhibits the high strength and stiffness along the fiber direction but provides the minimal transfer of these properties in the transverse direction. Since these matrix cracks often align with the central plane of the laminate, they are commonly referred to as transverse cracks. While matrix cracking may not be the primary factor leading to structural failure, it can significantly weaken the material strength and further affect the structural integrity. In order to maximize the load-carrying capability of a PMC laminate, designers must count for matrix cracking, as it often precedes the final failure of the structure [3-5,10,18,19,41].

Matrix cracking in PMC laminates can be divided into three sequential stages, i.e., crack initiation, growth, and final localization, culmination in the ultimate failure. Furthermore, intralaminar crack initiation within a ply (lamina) is influenced by various factors, e.g., the laminate stacking sequence and material properties. In the design of composite structures, lamination optimization is often employed, where the arrangement of plies determines the overall stiffness and the failure behavior of the PMC structure. While cross-ply composite laminates with plies oriented at 0 and 90 degrees offer a straightforward lamination configuration, more complex loading conditions require intricate lamination arrangements. The stiffness of the plies and the entire laminate of a PMC decreases as damage accumulates. The decrease in stiffness can be associated with multiple factors, e.g., the density of intralaminar cracks, the level of delamination, or a combination of both, etc. [19].

2.2. Current Understandings

The initial investigations of microcracking within a PMC laminate involved use of cross-ply laminates composed of UD polyester reinforced with glass fibers [20] and epoxy reinforced with glass fibers [21]. In the scenario that involved thick plies positioned at a 90-degree angle, the initiation of transverse microcracks occurred at the edges of the specimen and thereafter progressed rapidly over the entire width of the cross-section. This phenomenon of edge cracking was also observed in thinner plies. Notably, the tensile strain required for initiation of transverse cracks exhibited an increasing trend as the thickness of the 90-degree plies decreased [22]. It was observed that for extremely thin plies with the thickness of less than 0.1 mm, transverse crack did not initiate, and instead, laminate failure occurred. The explanation for such thickness-dependent behavior was subsequently made by Talreja [23], who attributed it to the constraint exerted by the uncracked plies on the cracked plies. As the thickness of the 90-degree plies increased, the constraint arising from the 0-degree plies diminished, resulting in the initiation of microcracking at lower applied strains, and conversely, thinner plies experienced crack initiation at higher strains. A microscopic examination aimed at understanding the origin of microcracks revealed their correlation to the processing defects, voids, and regions with a higher fiber volume fraction [21]. These microcracks typically initiated with the debonding of the fiber-matrix interface. George et al. [24,25] in their series of two papers also reported that the global tensile strength of a PMC laminate is increased significantly with the decrease of ply thickness in thin constrained plies while the global strength of thick plies were almost remained constant.

The initial concept of the first-ply failure (FPF) hypothesis was proposed by Hahn and Tsai [12] to estimate the strain necessary to trigger the first microcracking Figure 2.4. The underlying principle of this theory assumes that the first cracking occurs when the strain

undergoing within the plies reaches a certain threshold, evolving the onset of cracking. Nevertheless, these predictions were not according to empirical data. This theory does not consider the ply thickness of the PMC laminates. The deviation from the experimental findings is obvious. Subsequent efforts to refine this theory by incorporating all the stress components were unsuccessful [10].

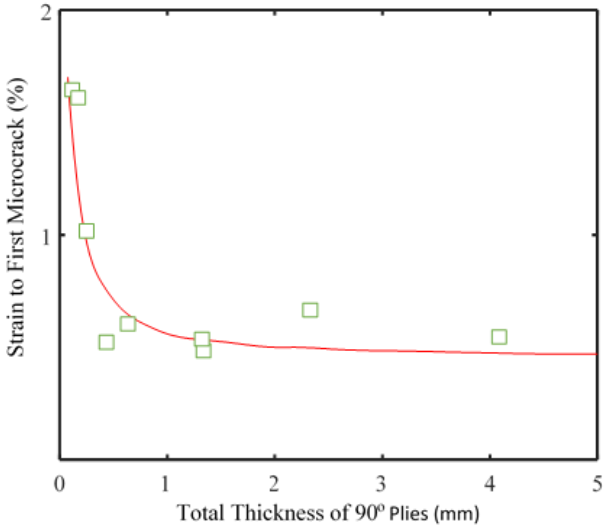

Figure 2.4 Strain to induce transverse cracking in 90-degree plies with varying thickness in a cross-ply PMC laminates [Reproduced from [10,22]].

In the case that matrix cracking is the predominant failure mode in a PMC laminate, it is common that the PMC laminate exhibits an enhanced capacity to support higher loads without an immediate reduction in its ability to transfer loads. Despite potential deviations in certain material properties, e.g., Young's modulus and coefficient of thermal expansion, the laminate is capable of retaining its load-carrying capacity. Allowing for controlled damage within a composite laminate can lead to more efficient design strategies. However, this methodology requires a thorough understanding of the mechanisms governing the crack initiation and progression, as well as their subsequent influences on the mechanical properties of the PMC

laminates. Multiple instances of crack initiation can yield several adverse consequences as reported by Arbate [18] as follows:

- The presence of cracks in plies leads to a decrease in the effective stiffness, which in turn causes stress redistribution within the PMC structure.
- Changes in the coefficients of thermal expansion of the PMC laminate.
- The initiation of delamination between plies or the failure of fibers in the 0-degree plies.
- The facilitation of fluid seepage in pressure vessels and heightened vulnerability to moisture infiltration are among the various adverse consequences.

The study of transverse ply cracking in PMC laminates has been a subject of continuous research for decades, which is aimed at a comprehensive understanding of its mechanics and influence in the mechanical behavior of PMC laminates. One can refer to the following references [24-28] to additional understand the early stage development of progressive cracking in cross-ply PMC laminates subjected to monotonically increasing loads. To date, several effective models have been developed in the literature for prediction of progressive cracking in composite laminates. These models include the ply discount method, various adaptations of the shear-lag model, a variational approach based on the minimization of complementary strain energy, the continuum damage mechanics approach, an efficient experimental technique, and numerical methods, e.g., those based on FEM [10,18,19].

Within the context of energy-based models, microcrack initiation occurs whenever the accumulated strain energy becomes sufficient to surpass the critical energy release rate for crack growth. This criterion for crack initiation and propagation is rooted in the principles of classical linear elastic fracture mechanics (LEFM). In contrast to LEFM, transverse cracking entails the

creation of a measurable quantity of additional fracture area. When utilized in conjunction with precise stress analysis techniques, e.g., the stress-function variational method and FEM, it is anticipated that this approach would produce more accurate predictions of crack growth in various cross-ply PMC laminates [51,52].

However, according to the classical strength theory, cracking occurs when the stress level reaches the transverse tensile strength of the ply material or satisfies a failure criterion based on a multi-axial stress state. The model above was unsuccessful in accurately identifying the onset and advancement of cracks across various ply thicknesses. Moreover, the applicability of these models is severely restricted to cross-ply laminates due to the requirement for comprehensive stress analysis. Yet, their predictions have the difficulty to align with experimental measurements [53].

Below an overview of the main research endeavors aimed at modeling the matrix cracking in PMC laminates is presented. Table 2.1 lists a few typical methods that were used to predict the stresses and matrix cracking in composite laminates.

2.2.1. Ply discount method

In this method, the stiffness of cracked plies is ignored, which makes it easier to model the matrix cracking. However, this approach tends to underestimate the stiffness of the laminate that have cracks, as the cracked plies can still contribute significantly to the load-carrying capacity [29]. As an alternative approach, the modified ply-discount model essentially assigns a transverse stiffness value of zero to the plies that have experienced cracks, which can be more effective. These models do not account for variations in stiffness due to crack density and are better suited for situations with high crack densities. With their simplicity, these models often

lack the reliability in design and failure analysis due to their reliance on a coarse assessment of the effects of transverse cracking.

2.2.2. Variational approach

In their study, Hashin [30,31] utilized the minimal complementary potential energy theory to predict the ply stresses stiffness, and coefficients of thermal expansion of cross-ply laminates that contain evenly distributed ply cracks. The approach utilized in this study entails the solving of a 2D boundary value problem and offers superior performance compared to one-dimensional (1D) shear-lag approaches. The predicted results based on this method demonstrated excellent agreement with experimental data. However, when it comes to analyzing the stresses in more general composite laminate configurations other than cross-ply laminates, particularly off-axis layups, the variational technique faces significant challenges, and at now, no variational solution is available for laminates of this nature [10]. This limitation indicates a major drawback of the variational approach. Figure 2.5 depicts the primary unit cell employed in the solving of the resultant 2D boundary value problem concerning cracked cross-ply laminates [32].

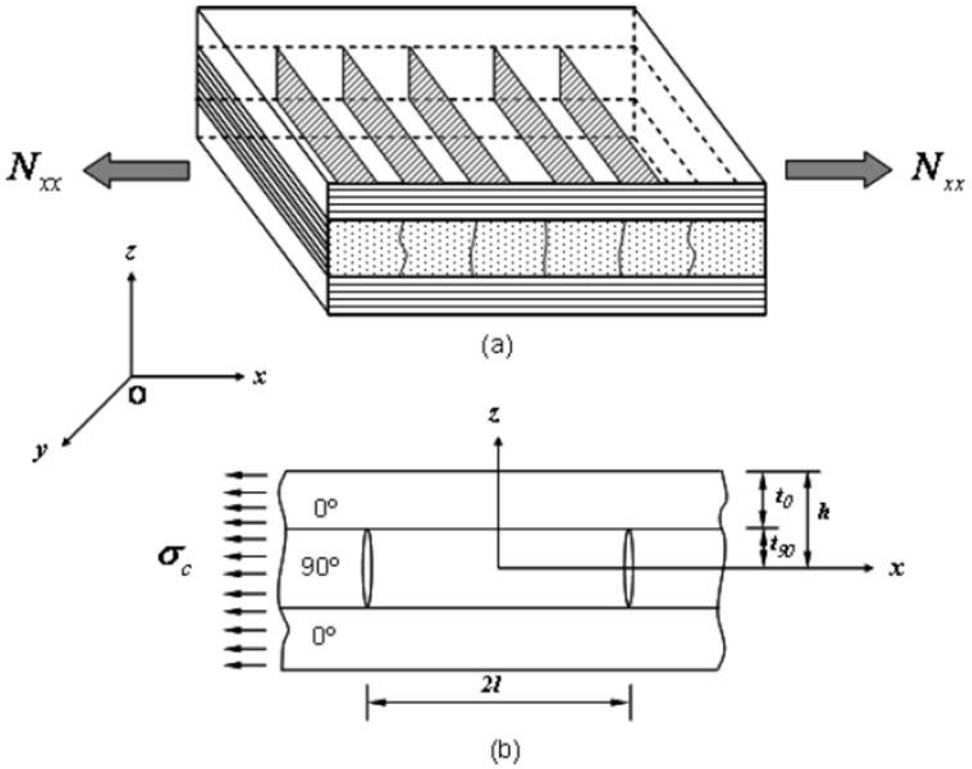

Figure 2.5 The boundary value problem pertaining to a cross-ply composite laminate with a crack [32].

Hashin [29] assumed that the normal stresses in the load direction remain constant throughout the ply thickness. Additionally, the stress field is formulated in such a way that it satisfies the stress equilibrium as well as boundary and interface conditions via minimizing the complementary strain energy of the laminate. The following ODE is obtained with Hashin's variational scheme as

$$\frac{d^4\varphi}{d\zeta^4} + p\frac{d^2\varphi}{d\zeta^2} + q\varphi = 0, \tag{2.1}$$

where $\zeta = \frac{x}{t_{90}}$, and p and q are two laminate parameters, φ is a function that describes the stress disturbance resulting from cracking. The relationship between the longitudinal stress in the 90° ply and φ is given by

$$\sigma_{xx}^{90} = \sigma_{xx0}^{90}[1 - \varphi(x)], \tag{2.2}$$

where σ_{xx}^{90} is the 90° ply normal stress before cracking. In addition, the semi-analytic method proposed by McCartney [33] involves utilizing a generalized plane strain formulation. This approach assumes that two distinct functions determine the in-plane typical stress dependency on the two in-plane coordinates. In order to adequately represent the variation in stress over the thickness of a ply, it is the common practice to partition the ply into multiple thin sub-plies. The equilibrium equations are then applied using the average stress fields within each sub-ply. The process results in a series of recursive equations, rendering this method semi-analytic and requiring numerical calculations.

2.2.3. Continuum damage mechanics (CDM)

Using principles of damage mechanics presents a viable alternative method for characterizing the mechanical behavior of PMC laminates with matrix cracking. In continuum damage mechanics, specific parameters must be calibrated using experimental or numerical data. In a study conducted by Lee et al. (34), an empirical correlation was established between the internal damage state parameter and the stiffness of a matrix-cracked cross-ply laminate. These researchers utilized minimum potential energy theory to calculate the approximate solutions for the local stresses and strains, facilitating determination of the upper bounds on the laminate stiffness.

The fundamental process involves quantifying damage using appropriate parameters and then formulating the governing equations that describe its progression and impact on the mechanical properties of the composite laminate. The first step in this process involves defining the damage and establishing an appropriate metric. This method commonly addresses defects with the size much less than the customary microscopic size of the material under the assumption that the material exhibits homogeneous on a macroscopic scale [18]. So far, researchers have formulated several models for stress and fracture analysis of PMC laminates to undergo transverse matrix cracking. However, this method may not be feasible in practice due to the extensive efforts required to extract the relevant data on crack dispersion. Additionally, application of this method would require interrupting the ongoing testing process.

2.2.4. Numerical methods

Various numerical methods have been employed to analyze cracked cross-ply PMC laminates. The majority of these analyses are focused on addressing the 2D boundary value problems, similar to Hashin's [30,31] variational approach, with the assumption of either plane stress or generalized plane strain states. Only a few have ventured into performing comprehensive 3D stress analyses. The main computational approaches employed in such study include FEM, finite difference method (FDM), boundary element method (BEM), and finite strip method (FSM) [10,18,19]. These methods provide the benefit of yielding more precise stress solutions, hence offering significantly improved insights. For example, Marek [35] studied the mechanical response of UD fiber-reinforced PMCs subjected to transverse tension. This investigation included numerical homogenization techniques based on FEM. The model above demonstrates the high accuracy in simulating the damage procedure. The numerical outcomes

indicate that deviations in the local fiber orientation significantly contribute to the crack initiation in matrix due to stress concentration. However, it is important to note that these methods are often application-specified, as they require reconfiguration whenever changes exist in the laminate construction, material, or crack density. As a matter of fact, any analytical methods, whether existing, proposed, or under development, are frequently subjected to verification, comparison, or validation through various computational means.

Table 2.1 Comparison of different methods used to model the matrix cracking in PMC laminates

Method	Description	Advantages	Limitations
Ply discount method	Empirical approach where the cracked plies are assumed to carry reduced loads due to matrix cracking.	Gives simple and quick analysis.	Oversimplifies complex damage mechanisms.
Variational approach	Utilization of variational principles to find approximate solutions to the governing equations of cracked laminates.	Provides analytical insights into crack behavior.	Limited to specific problems with known analytical solutions.
Continuum damage mechanics	Numerical modeling approach that simulates the crack initiation and growth in composite materials.	Captures crack evolution over time.	Requires detailed material properties and data.
Numerical methods	Use of FEM or BEM to solve the governing equations for stress and strain in composite laminates.	Offers accurate and versatile analysis for PMC laminates of complex geometries.	Requires expertise in numerical modeling and software.
Shear-lag model	Analytical method to analyze the gradual load transfer between intact and cracked regions in a PMC laminate.	Provides insights into stress distribution in PMC laminates.	Complex calculations for general laminate configurations.

2.2.5. Shear-lag model

The shear-lag model is a widely employed analytical approach to examine the stresses in a multilayered composite and progressive matrix cracking in composite laminates. Shear-lag analyses in composite materials research often involve numerous approximations. This method considers the impact of load transfer between microcracked plies and their neighboring plies. This model assumes that load transfer between plies primarily occurs in shear layers located between adjacent plies. By closely examining the existing analytic and semi-analytic models [24-28,35-36] of progressive cracking in cross-ply PMC laminates, it has been observed that oversimplified mechanical models have been utilized to calculate the interfacial stresses at the ply surfaces in cross-ply laminates, in which the plies are simplified as tension rods and shear-lag model is adopted for determining the shear stress at ply surfaces. This assumption suggests that neighboring plies always experience the same normal stress in the direction of the external load. The specific characteristics of the shear layers, e.g., the length and stiffness, are not precisely defined. The shear-lag hypothesis does not consider the stress and strain variations across the ply thickness.

All shear-lag analyses universally incorporate an assumption that simplifies the in-plane shear stress, represented as τ_{xy}, by separating it into the *x* and *y* axes. Decoupling reduces the 2D-planar elasticity problems to a more manageable 1D problem. The conventional simplification pertaining to shear stress involves the assumption that [37]

$$\tau_{xy} \propto \frac{\partial v}{\partial x}, \tag{2.3}$$

where the variable *v* denotes the displacement in the *y*-direction. Within the context of linear elasticity, shear stress τ_{xy} is expressed

$$\tau_{xy} = G_{xy}\gamma_{xy} = G_{xy}\left(\frac{\partial v}{\partial x} + \frac{\partial u}{\partial y}\right), \tag{2.4}$$

where G_{xy} is the in-plane shear modulus, γ_{xy} represents the in-plane shear strain, and *u* denotes the displacement in the *x*-direction. The fundamental assumption underlying all shear-lag analyses is that

$$\frac{\partial u}{\partial y} = 0, \text{or at least that } \left|\frac{\partial u}{\partial y}\right| \ll \left|\frac{\partial v}{\partial x}\right| \tag{2.5}$$

Given 1D nature, doubts exist about the applicability of shear-lag model to more general layup configurations beyond the simple cross-ply composites. Researchers have made efforts to refine this model, and successful applications have been achieved in cross-ply laminates. Some shear-lag models have also incorporated crack interactions into their procedure [19].

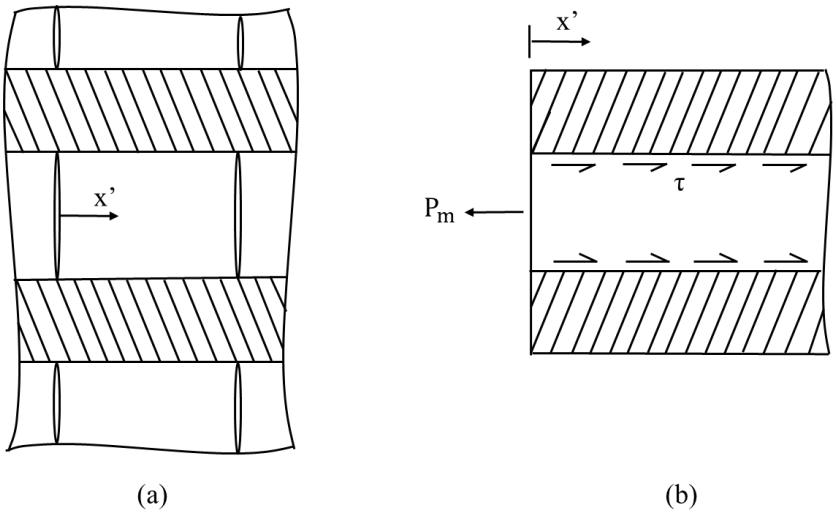

Figure 2.6 A representative cross-section of a cracked PMC laminate and a representative area element in load equilibrium [Reproduced from [38]]

Aveston et al. [38] employed the shear-lag approach to examine the failure process of fibrous composite materials characterized by a brittle matrix that exhibits a lower failure strain

compared to that of the reinforcing fibers. They focused on the matrix cracking between the stiff reinforcing fibers, with the assumption of complete fiber debonding between two adjacent cracks. The criteria for multiple matrix cracking were identified by Aveston et al. [38] such that matrix stress equals to or exceeds the failure stress, and the energy consumption matches or is less than the energy supply during the transition from an uncracked state to the one with a single crack spanning the entire specimen. Hence, the governing equation can be written as,

$$2\gamma_m V_m + \gamma_{db} + U_s + \Delta U_f \leq \Delta W + \Delta U_m, \tag{2.6}$$

where γ_m is the surface energy per unit area of the crack, V_m is the matrix volume fraction, γ_{db} is the interface energy per unit area between fiber and matrix, U_s is the work done by matrix sliding unit cross-sectional area A over a distance $2x'$ on the fiber surface, ΔU_f is the increase of elastic strain energy of the reinforcing fibers per A (with unit thickness), ΔW is the work done by external (fixed) load per A (with unit thickness), and ΔU_m is the reduction of elastic strain energy of matrix per A (with unit thickness). Aveston et al. [38] derived an expression to the strain neglecting the contribution of γ_{db} as

$$\varepsilon_{muc} = \left(\frac{12\tau\gamma_m E_f {V_f}^2}{E_c E_m^2 r V_m}\right)^{1/3}, \tag{2.7}$$

where E_f and E_r are the Young's moduli of the reinforcing fiber and polymeric matrix, respectively. According to Aveston and Kelly [39] in the extension of their previous work, they formulated an ODE for the load transfer such that

$$\frac{d^2(\Delta\sigma)}{dy^2} = \phi\Delta\sigma, \tag{2.8}$$

where

$$\phi = \frac{HE_c}{E_f E_m V_m}, \tag{2.9}$$

with E_c as the Young's modulus of the composite and *H* as a constant. In their approach to solving *H,* Aveston and Kelly made an unreasonable assumption of a constant σ_y, thereby violating the underlying assumption that σ_y is dependent on *y*.

The modified shear-lag technique presented by Lim et al. [40] introduces the concept of a thin interlaminar shear layer between the cracked and intact ply group. This layer is responsible for transferring the load, as opposed to the entire 90^o ply group. They applied the Griffith energy balance criterion. However, it is necessary to make some assumptions concerning the thickness and shear modulus of the shear layer in this analysis. The matrix cracking problem was addressed by Tan et al. [27] by utilizing an approximate 2D elasticity solution and fracture mechanics. The formulated ODE is the same as Eq. (2.8), and numerous investigations have been adopted to address the issue of transverse cracking based on the shear-lag method. The common feature of these studies is that the same ODE (Eq. 2.8) was examined, with the primary distinction among them lying in how the shear-lag parameters are determined.

Consequently, similar to the stress results obtained through the shear-lag model in the literature, the shear stress along the ply surfaces fails to conform to the traction-free condition near crack tips and free edges. Moreover, the normal stresses perpendicular to the ply direction are completely disregarded, meaning that the deformation of the plies in the transverse plies is not considered. Consequently, stress analysis of these fiber-reinforced PMC laminates can be characterized as somewhat flawed, potentially leading to noticeably deviation in the stress distribution in the PMC laminates.

2.3. Stress-function Variational Method

All the methods reviewed above have certain limitations for prediction of the interfacial stresses of PMC laminates with progressive cracking. To effectively overcome the drawbacks of these existing models for interfacial stress analysis in PMC laminates as well as bonded and adhesively bonded joints, a high-efficiency and accurate semi-analytic stress-function variational method was formulated by Wu and his group [12-16]. This stress-function variational method was initially formulated to find the free-edge interfacial stresses in bonded and adhesively bonded joints. It was later extended to predict the progressive cracking in hard surface coatings.

This method uniquely introduces two unknown functions for the interfacial shear and normal stresses on each interface of the joints, which are further used to determine all the planar stress components in each adherend of the joints. The assumption made in this method is that the axial normal stress within each adherend of the joints varies linearly across the adherend layer. The unknown interfacial stress functions are further used to express the planar shear and transverse normal stresses in the adherends via evoking the static equilibrium equations in 2D elasticity. In this approach, the stress continuity across the adherend interfaces and the traction BCs at both the upper and lower surfaces and the free ends of the adherends can be exactly satisfied. The unknown interfacial stress functions are determined via triggering the minimum complementary strain energy theorem, which results in two coupled governing ODEs of the two unknown interfacial stress functions in the case of bonded joints with two adherends and finally solved explicitly in terms of eigenfunctions to satisfy all traction BCs at free edges. The interfacial shear and normal stresses predicted by this method are in high accuracy as validated by detailed FEA.

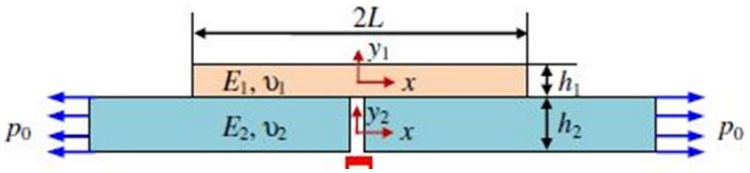

(A)

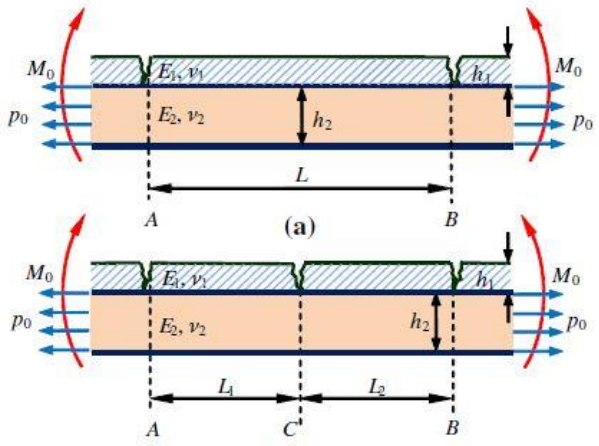

(B)

Figure 2.7 *(A).* Schematic of a single-sided strap joint consisting of a slender cover layer bonded to two identical slender substrate layers and *(B).* (a) Through-thickness cracking in a coating layer of a brittle thin-film/substrate system, (b) formation of a secondary crack [12,15].

With the same approach, the stress-function variational method is subsequently employed for predicting the free-edge interfacial stresses in adhesively bonded joints. In their paper, Wu et al. [15] further formulated a simple semi-analytic strain energy method to analyze the interfacial stresses and progressive cracking in surface coatings within the framework of LEFM, with taking into account of the combination of tensile traction, bending moment, and temperature change. This semi-analytic approach has been proven to be highly accurate and efficient and satisfies all the traction BCs.

With the above literature review, the primary objective of this thesis is to expand the stress-function variational method to accurately analyze the interfacial stresses in PMC laminates

with progressive cracking. Numerical solutions based on FEM (ANSYS^{TM}) are used to validate the present approach. During the process, without loss of the generality, a three-layered symmetric cross-ply PMC laminate is considered, and two unknown interfacial shear and normal stress functions are adopted at each ply surface. The planar stress field in each ply of the laminate is expressed in terms of these unknown interfacial stress functions. The axial normal stress in each ply is assumed to vary linearly across the ply thickness following the flexural stress formula of classic Euler-Bernoulli beams, i.e., treating the laminate plies as elastic beams rather than simple tension bars as used in existing literature. The remaining planar shear and transverse normal stresses in each ply are determined via triggering the static equilibrium equations within the framework of 2D elasticity and traction BCs at the top and bottom surfaces of the laminate and at the crack surfaces of the plies after cracking.

A set of two coupled ODEs for the two unknown interfacial stress functions is obtained by evoking the theorem of minimum complementary strain energy of the representative segmental PMC laminate. These ODEs are then solved explicitly in terms of eigenfunctions to satisfy the proper traction BCs. This method ensures that the stress field in the plies satisfies all the traction BCs, especially the shear-free conditions at the crack tips, which were typically ignored in many analytic methods reported in the literature.

The accuracy and effectiveness of the stress-function variational method are validated by comparing the interfacial stresses of the PMC laminate with those predicted by FEM and other analytical methods. Additionally, dependencies of the interfacial stresses and crack spacing on the laminate geometries, elastic properties, and temperature changes are examined.

The remaining chapters of the thesis are organized as follows:

Chapter 3 provides the theoretical framework of the stress-function variational method for accurate interfacial stress analysis of a three-layered symmetric cross-ply composite laminate subjected to uniaxial tension. The obtained stress field in the plies is used to determine the strain energy release rate after transverse cracking in the mid-ply and to predict the crack spacing in the composite laminate. In addition, scaling analysis is conducted to examine how interfacial stresses and crack spacing depend on the laminate geometries and elastic properties. Comparisons are made between the present results and those predicted by FEM and available in the literature.

Chapter 4 focuses on the interfacial stress analysis of adhesively bonded circular joints by detailed FEA.

Chapter 5 summarizes the current work and outlines the potential future research directions after the present thesis work.

3. STRESS-FUNCTION VARIATIONAL METHOD FOR ANALYSIS OF INTERFACIAL STRESSES AND PROGRESSIVE CRACKING IN COMPOSITE LAMINATES

This chapter is to formulate a stress-function variational method for analyzing the interfacial stresses and progressive cracking in a three-layered cross-ply composite laminates subjected to uniaxial tension. This new semi-analytical method can explicitly represent the entire stress field in composite laminates by adopting the standard procedure of the stress-function variational method. The stress results predicted by this method can be effectively validated by using the commercial FEA software package (ANSYS®) as demonstrated in this chapter.

3.1. Problem Formulation and Solution

Without loss of the generality, consider a three-layered symmetric cross-ply composite laminate subjected to uniaxial tension as shown in Figure 3.1. This classic laminate model has been adopted for progressive cracking analysis with the interfacial stresses determined by the shear-lag model in the literature. Herein, the upper and lower plies of this cross-ply composite laminate are identical, UD composite plies with the reinforcing fibers in the longitudinal direction, while the mid-ply of the laminate is a transverse ply with the reinforcing fibers aligned in the transverse direction. For the convenience of the upcoming discussions, the upper and lower plies are treated as homogeneous, isotropic, linearly elastic material with Young's modulus E_1, Poisson's ratio υ_1, and ply thickness h_1; the mid-ply is also treated as homogeneous, isotropic, linearly elastic material with Young's modulus E_2, Poisson's ratio υ_2, and ply thickness $2h_2$. With the assumption that the length and width of the laminate are large compared to the transverse dimensions, the 3D free-edge effects can be safely excluded. Thus, the stress analysis of this composite laminate can be reduced to a plane problem as shown in Figure 3.2 (a), either in plane-stress or plane-strain state depending on the lateral constraint conditions.

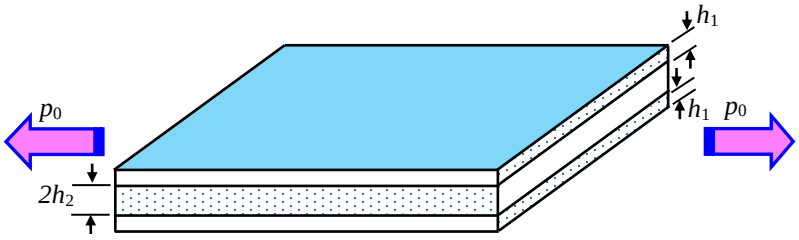

Figure 3.1 Schematic diagram of a three-layered symmetric cross-ply composite laminate subjected to uniaxial tension.

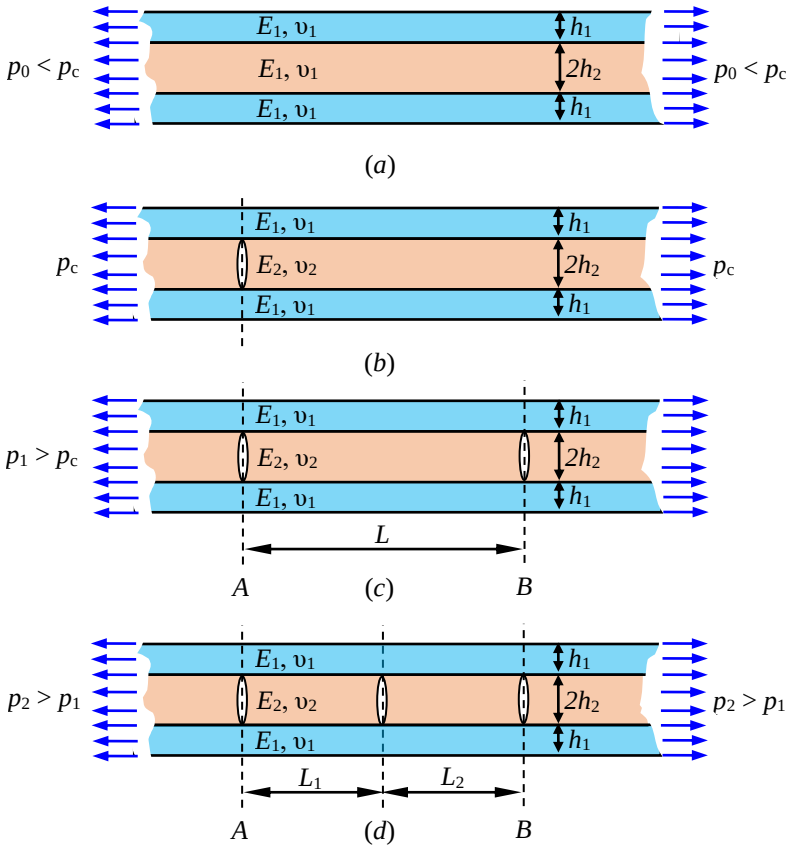

Figure 3.2 Schematic progressive transverse cracking in a three-layered symmetric cross-ply composite laminate subjected to uniaxial tension. (a) No crack for the initial effective axial stress $p_0 < p_c$ (the critical effective axial stress level to trigger cracking initiation), (b) crack initiation (first crack to appear) for the effective axial stress reaching p_c, (c) periodic transverse cracks with spacing L for the effective axial stress $p_1 > p_c$, and (d) periodic transverse cracks with increasing dimensionless crack spacing $2h_2/L$ for increased effective axial stress $p_2 > p_1 > p_c$.

In the Figure 3.2, p_0 represents the initial effective axial stress, p_c the critical effective axial stress level to trigger cracking initiation, and $p_1$and p_2 are two increased effective axial stresses to lead to periodic cracking. When the composite laminate is subjected to monotonically increasing uniaxial tension, the first transverse cracking likely initiates in the mid-ply that carries the low ultimate tensile strength due to the brittleness of the typical thermosetting resins as well as the reinforcing fibers in the transverse direction as illustrated in Figure 3.2 (b). With further increasing the axial stress level, periodic cracks appear with gradually increasing crack density as illustrated in Figures 3.2 (c) and 3.2 (d), i.e., progressive cracking. In addition, the upper and lower plies carry the coefficient of thermal expansion different from that of the mid-ply due to different orientations of the reinforcing fibers. Thus, temperature change will induce different thermal strains and stresses in the plies that further influence the progressive cracking. For the convenience of the study, only axial tension loading is considered.

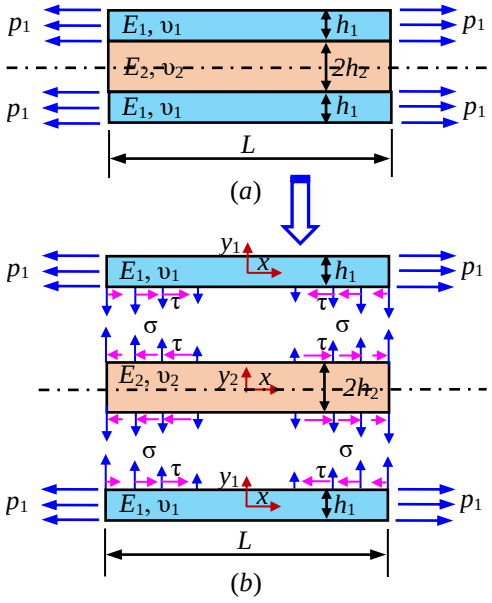

Figure 3.3 (a) Schematic diagram of a representative segment of a three-layered symmetric cross-ply composite laminate between two neighboring cracks, and (b) schematic symmetric interfacial shear and normal stresses at the upper and lower interfaces of the laminate.

3.1.1. Static equilibrium equations

For the present three-layered composite laminate subjected to uniaxial tension, periodic cracking is triggered in the mid-ply once the effective tensile stress is higher than the critical value p_c as shown in Figs. 3.2 (c) and 3.2 (d). After periodic cracking, the laminate plies near the crack tips are in the general planar stress state. The plies of the composite laminate are slender and can be treated as the classic Euler-Bernoulli beams for simplification of the stress analysis while still maintaining sufficient accuracy. Consider a representative periodic laminate segment with the crack spacing L as shown in Fig. 3.3 (a). Due to symmetries of the laminate configuration and the applied axial loads, the interfacial normal and shear stresses at the upper and lower interfaces of the laminate are identical as illustrated in Fig. 3.3 (b). Thus, stress analysis of the laminate can be simplified to only analyze the stress field in the upper and middle plies. For the convenience of stress analysis, two coordinate systems of (x, y_1) and (x, y_2) are introduced to the upper and middle plies of the composite laminate, respectively, as shown in Fig. 3.3 (b), with *x*-axis along the mid-plane of each ply and *y*-axis passing through the perpendicular midline of the laminate segment.

Free-body diagrams (FBDs) of the representative segments of the upper and middle plies are shown in Figs. 3.4(a) and 3.4(b), respectively, in which the stress components and related stress resultants, i.e., the axial force S_{i}, shear force Q_{i}, and bending moment M_{i} (i = 1, 2) per unit width, are defined to follow the positive sign conventions as designated in elementary mechanics of materials. The equations governing the static equilibrium of a representative segmental element in the upper ply, expressed in terms of stress resultants, are as follows:

$$\Sigma F_x = 0: \frac{dS_1}{dx} = -\tau, \tag{3.1}$$

$$\Sigma F_y = 0: \frac{dQ_1}{dx} = -\sigma, \tag{3.2}$$

$$\Sigma M = 0: \frac{dM_1}{dx} = Q_1 - \frac{h_1}{2}\tau. \tag{3.3}$$

The static equilibrium equations for the representative segmental element of the mid-ply, as depicted in Figure 3.4(b), are as follows:

$$\Sigma F_x = 0: \frac{dS_2}{dx} = 2\tau, \tag{3.4}$$

$$\Sigma F_y = 0: \frac{dQ_2}{dx} = 0, \tag{3.5}$$

$$\Sigma M = 0: \frac{dM_2}{dx} = Q_2. \tag{3.6}$$

Figure 3.4(b) shows that the stress state of the mid-ply is simple due to the symmetric normal and shear stresses induced at the upper and lower interfaces.

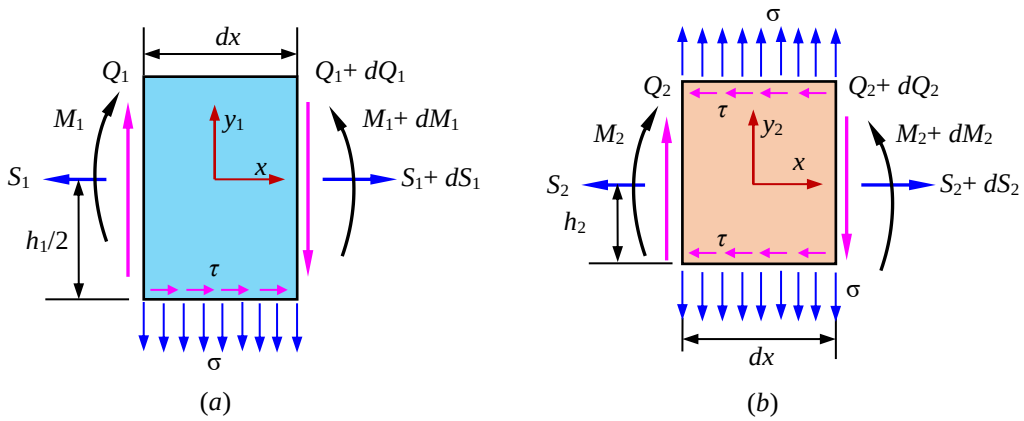

Figure 3.4 Free-body diagrams (FBDs) of the representative segmental elements of the three-layered symmetric cross-ply composite laminate. (*a*) FBD of the upper ply with interfacial normal and shear stresses at the lower surface and (*b*) FBD of the mid-ply with the symmetric interfacial normal and shear stresses at the upper and lower surfaces.

3.1.2. Stress resultants in plies

The symmetric shear and normal stresses at the upper and lower interfaces of the three-layered composite laminate under consideration as two unknown interfacial stress functions defined as

$$\tau = f(x) \text{ and } \sigma = g(x). \tag{3.7}$$

The shear-free conditions at the crack tips (edges) at x = -L/2 and L/2 can be expressed as

$$f(-L/2) = f(L/2) = 0. \tag{3.8}$$

In addition, the axial tractions, shear-forces and bending moments at the segmental ends of the laminate specify the traction BCs as

$$S_1(-L/2) = p_1 h_1, \tag{3.9a}$$

$$S_1(L/2) = p_1 h_1, \tag{3.9b}$$

$$Q_1(-L/2) = 0, \tag{3.9c}$$

$$Q_1(L/2) = 0, \tag{3.9d}$$

$$M_1(-L/2) = 0, \tag{3.9e}$$

$$M_1(L/2) = 0, \tag{3.9f}$$

$$S_2(-L/2) = 0, \tag{3.9g}$$

$$S_2(L/2) = 0, \tag{3.9h}$$

$$Q_2(-L/2) = 0, \tag{3.9i}$$

$$Q_2(L/2) = 0, \tag{3.9j}$$

$$M_2(-L/2) = 0, \tag{3.9k}$$

$$M_2(L/2) = 0. \tag{3.9l}$$

In the aforementioned context, it is worth noting that not all the traction BCs are linearly independent, as to be discussed later.

In the case of thermomechanical stress analysis of the composite laminate due to a pure uniform temperature change ΔT and without constraints at boundaries, the right terms of (3.9a) and (3.9b) are set as zeros to satisfy the traction-free BCs.

Furthermore, all the stress resultants of the segmental elements of the plies can be expressed in terms of the two unknown interfacial stress functions *f* and *g* as adopted in (3.7). By integrating (3.1) with respect to *x* from *x* = -*L*/2, it yields

$$\int_{-L/2}^{x} dS_1 = -\int_{\frac{L}{2}}^{x} f(\xi)d\xi. \tag{3.10}$$

With the shear-free condition at *x* = -*L*/2, i.e., BCs (3.7) and (3.9), the axial normal force $S_1(x)$ in the upper ply can be determined from Eq. (3.10) as

$$S_1(x) = p_1 h_1 - \int_{-\frac{L}{2}}^{x} f(\xi)d\xi. \tag{3.11}$$

By performing integration (3.2) with respect to x from *x* = -*L*/2, the shear force of the upper ply as

$$\int_{-L/2}^{x} dQ_1 = -\int_{-\frac{L}{2}}^{x} g(\xi)d\xi. \tag{3.12}$$

With the assistance of the shear-free condition at *x* = -*L*/2 as given in (3.9c), the shear force $Q_1(x)$in the upper ply can be determined from (3.12) as

$$Q_1(x) = -\int_{-\frac{L}{2}}^{x} g(\xi)d\xi. \tag{3.13}$$

Now, integrating (3.3) with respect to *x* from *x* = -*L*/2 results in

$$\int_{-L/2}^{x} dM_1 = \int_{-L/2}^{x} [Q_1(\xi) - \frac{h_1}{2}\tau]d\xi. \tag{3.14}$$

By utilizing the bending-moment BC at *x* = -*L*/2 as provided in (3.9e), the bending moment $M_1(x)$ in the upper ply can be solved from (3.14) as

$$M_1(x) = -\int_{-\frac{L}{2}}^{x}\int_{-\frac{L}{2}}^{\xi} g(\varsigma)d\varsigma d\xi - \frac{h_1}{2}\int_{-\frac{L}{2}}^{x} f(\xi)d\xi. \tag{3.15}$$

Based on the same procedure, integrating (3.4) with respect to *x* from *x* = -*L*/2 yields

$$\int_{-L/2}^{x} dS_2 = \int_{-L/2}^{x} f(\xi)d\xi. \tag{3.16}$$

By implementing the axial traction BC at x = -L/2 as specified in (3.9g), the axial force $S_2(x)$ in the mid-ply can be determined from (3.16) as

$$S_2(x) = 2\int_{-\frac{L}{2}}^{x} f(\xi)d\xi. \tag{3.17}$$

In addition, the shear-force $Q_2(x)$ and bending moment $M_2(x)$of the mid-ply can be calculated by integrating (3.5) and (3.6) with respect to x, ranging from x = -L/2:

$$Q_2(x) = 0, \tag{3.18}$$

$$M_2(x) = 0. \tag{3.19}$$

In the previous discussion, the derivations have incorporated two BCs relating to the absence of shear force and bending moment at the position x = -L/2, as stipulated in Eqs. (3.9i) and (3.9k).

3.1.3. Planar stresses in the three-layered composite laminate

3.1.3.1. Planar stresses in the upper ply

For linearly elastic slender plies of the composite laminate under consideration, the axial normal stress in each ply can be assumed to vary linearly across the ply thickness. The axial stress can be calculated by applying the flexural stress formula of classic Euler-Bernoulli beams as

$$\begin{aligned}\sigma_{xx}^{(1)} &= \frac{S_1}{h_1} - \frac{M_1 y_1}{I_1} \\ &= p_1 - \frac{1}{h_1}\int_{-\frac{L}{2}}^{x} f(\xi)d\xi + \frac{12y_1}{h_1^3}\left[\int_{-\frac{L}{2}}^{x}\int_{-\frac{L}{2}}^{\xi} g(\varsigma)d\varsigma d\xi + \frac{h_1}{2}\int_{-\frac{L}{2}}^{x} f(\xi)d\xi\right].\end{aligned} \tag{3.20}$$

Shear stress $\tau_{y_1x}^{(1)}$ in the upper ply of the laminate can be solved by integrating the 2D equilibrium equation:

$$\frac{\partial \sigma_{xx}^{(1)}}{\partial x} + \frac{\partial \tau_{y_1x}^{(1)}}{\partial y_1} = 0, \tag{3.21}$$

with respect to coordinate y_1 from an arbitrary location *y* to the top surface at y_1=h_1/2:

$$\int_{y_1}^{h_1/2} \frac{\partial \sigma_{xx}^{(1)}}{\partial x} dy_1 + \int_{y_1}^{h_1/2} \frac{\partial \tau_{y_1x}^{(1)}}{\partial y_1} dy_1 = 0, \tag{3.22}$$

which leads to

$$\tau_{y_1x}^{(1)} = -\frac{1}{h_1}\left[\left(\frac{h_1}{2} - y_1\right) - \frac{3}{h_1}\left(\frac{h_1^2}{4} - y_1^2\right)\right] f(x) + \frac{6}{h_1^3}\left(\frac{h_1^2}{4} - y_1^2\right) \int_{-\frac{L}{2}}^{x} g(\xi) d\xi. \tag{3.23}$$

In the above, traction-free BC: $\tau_{y_1x}^{(1)}(h_1/2) = 0$ has been employed. Furthermore, the transverse normal stress $\sigma_{y_1y_1}^{(1)}$ in the upper ply can be calculated by integrating the 2D equilibrium equation:

$$\frac{\partial \sigma_{y_1y_1}^{(1)}}{\partial y_1} + \frac{\partial \tau_{xy_1}^{(1)}}{\partial x} = 0, \tag{3.24}$$

with respect to y_1 from an arbitrary location *y* to the top surface at y_1=-h_1/2 as

$$\int_{y_1}^{h_1/2} \frac{\partial \sigma_{y_1y_1}^{(1)}}{\partial y_1} dy_1 + \int_{y_1}^{h_1/2} \frac{\partial \tau_{xy_1}^{(1)}}{\partial x} dy_1 = 0, \tag{3.25}$$

which yields

$$\sigma_{y_1y_1}^{(1)} = -\frac{1}{h_1}\left\{\frac{h_1}{2}\left(\frac{h_1}{2}-y_1\right)-\frac{1}{2}\left(\frac{{h_1}^2}{4}-{y_1}^2\right)\right.$$

$$\left.-\frac{3}{h_1}\left[\frac{{h_1}^2}{4}\left(\frac{h_1}{2}-y_1\right)-\frac{1}{3}\left(\frac{{h_1}^3}{8}-{y_1}^3\right)\right]\right\}f'(x) \tag{3.26}$$

$$+\frac{6}{{h_1}^3}\left[\frac{{h_1}^2}{4}\left(\frac{h_1}{2}-y_1\right)-\frac{1}{3}\left(\frac{{h_1}^3}{8}-{y_1}^3\right)\right]g(x).$$

In the process to derive (3.26), traction-free BC: $\tau_{y_1y_1}^{(1)}(h_1/2)=0$ has been carried out.

3.1.3.2. Planar stresses in the mid-ply

The stress components in the mid-ply can be approximated using the similar procedure. The axial normal stress can be approached by applying the flexural stress formula of classic Euler-Bernoulli beams and the stress resultants in the mid-ply (3.17-3.19):

$$\sigma_{xx}^{(2)} = \frac{S_2}{h_2} - \frac{M_2 y_2}{I_2} = \frac{2}{h_2}\int_{-\frac{L}{2}}^{x} f(\xi)d\xi. \tag{3.27}$$

Due to the symmetry of the composite laminate and external loading, no bending is exerted in the mid-ply and the axial normal stress does not vary across the ply thickness. Shear stress $\tau_{y_2x}^{(2)}$ can be calculated via integrating the 2D static equilibrium equation:

$$\frac{\partial\sigma_{xx}^{(2)}}{\partial x}+\frac{\partial\tau_{y_2x}^{(2)}}{\partial y_2}=0, \tag{3.28}$$

with respect to y_2 from the bottom surface $y_2=h_2/2$ to an arbitrary location $y_2$of the mid-ply as

$$\int_{-h_2/2}^{y_2}\frac{\partial\sigma_{xx}^{(2)}}{\partial x}dy_2+\int_{-h_2/2}^{y_2}\frac{\partial\tau_{y_2x}^{(2)}}{\partial y_2}dy_2=0, \tag{3.29}$$

which leads to

$$\tau_{y_2x}^{(2)} = \left[1 - \frac{2}{h_2}\left(y_2 + \frac{h_2}{2}\right)\right] f(x). \tag{3.30}$$

In the above, traction BC: $\tau_{y_2x}^{(2)}(-h_2/2) = f(x)$ has been carried out. Furthermore, normal stress $\sigma_{y_2y_2}^{(2)}$ in the mid-ply can be solved via integrating the 2D equilibrium equation:

$$\frac{\partial \sigma_{y_2y_2}^{(2)}}{\partial y_2} + \frac{\partial \tau_{xy_2}^{(2)}}{\partial x} = 0, \tag{3.31}$$

with respect to y_2 from the bottom surface at $y_2 = h_2/2$ to an arbitrary location y_2 as

$$\int_{-h_2/2}^{y_2} \frac{\partial \sigma_{y_2y_2}^{(2)}}{\partial y_2} dy_2 + \int_{-h_2/2}^{y_2} \frac{\partial \tau_{xy_2}^{(2)}}{\partial x} dy_2 = 0, \tag{3.32}$$

which further reduces to

$$\sigma_{y_2y_2}^{(2)} = g(x) - [\left(y_2 + \frac{h_2}{2}\right) - \frac{2}{h_2}\left[\frac{1}{2}\left(y_2^2 - \frac{h_2^2}{4}\right) + \frac{h_2}{2}\left(y_2 + \frac{h_2}{2}\right)\right] f'(x). \tag{3.33}$$

During the process to evaluate integral (3.32), traction BC: $\sigma_{y_2y_2}^{(2)}(-h_2/2) = g(x)$ has been evoked.

In the derivations above, when assuming that the axial normal stress changes linearly across the thickness of the ply, the shear and transverse normal stresses in the plies exhibit parabolic and cubic variations over the ply thickness, respectively, while being in static equilibrium.

3.1.4. Governing equations of interfacial stress functions and solution

With the stress components of the representative laminate segment as determined in Section 3.1.3, the total strain energy of the laminate segment ($-L/2 \leq x \leq L/2$) can be expressed as [12-16,40,42-44],

$$\mathrm{U}= 2\int_{-L/2}^{L/2}\int_{-h_1/2}^{h_1/2}\{\frac{1}{2}\left[\sigma_{xx}^{(1)}\varepsilon_{xx}^{(1)}+\sigma_{yy}^{(1)}\varepsilon_{yy}^{(1)}\right]+\frac{1+\upsilon_1}{E_1}(\tau_{y_1x}^{(1)})^2\}dxdy_1+$$
$$\int_{-L/2}^{L/2}\int_{-h_2/2}^{h_2/2}\{\frac{1}{2}\left[\sigma_{xx}^{(2)}\varepsilon_{xx}^{(2)}+\sigma_{yy}^{(2)}\varepsilon_{yy}^{(2)}\right]+\frac{1+\upsilon_2}{E_2}(\tau_{y_2x}^{(2)})^2\}dxdy_2. \quad (3.34)$$

In the above, $\varepsilon_{xx}^{(i)}$and $\varepsilon_{yy}^{(i)}$ (i = 1, 2) are respectively the axial and transverse normal strains of the plies, which are determined according to the generalized Hooke's law of isotropic, linearly thermoelastic substances in the plane-stress state as

$$\varepsilon_{xx}^{(i)}=\frac{1}{E_i}\sigma_{xx}^{(i)}-\frac{\upsilon_i}{E_i}\sigma_{yy}^{(i)}+\alpha_i\Delta T, \quad (3.35)$$

$$\varepsilon_{yy}^{(i)}=\frac{1}{E_i}\sigma_{yy}^{(i)}-\frac{\upsilon_i}{E_i}\sigma_{xx}^{(i)}+\alpha_i\Delta T. \quad (3.36)$$

In this context, α_i (i= 1, 2) represents the coefficients of thermal expansion for the upper and middle plies, and ΔT denotes the uniform temperature change of the laminate from a reference temperature of a thermomechanical-stress-free state. From a mathematical perspective, strain energy (3.34) is a functional in relation to the two unknown interfacial stress-functions *f* and *g*, as defined in (3.7). By applying the principle of minimum complementary strain energy of an elastic body, the strain energy of the composite laminate reaches the stationary point at the static equilibrium state. This indicates that the variation of strain energy (3.34) is zero [12-16,40,42-44],

$$\delta U=0, \quad (3.37)$$

i.e.,

$$\delta U = 2\int_{-L/2}^{L/2}\int_{-h_1/2}^{h_1/2}\{\frac{1}{2}\left[\sigma_{xx}^{(1)}\delta\varepsilon_{xx}^{(1)} + \delta\sigma_{xx}^{(1)}\varepsilon_{xx}^{(1)} + \sigma_{yy}^{(1)}\delta\varepsilon_{yy}^{(1)} + \delta\sigma_{yy}^{(1)}\varepsilon_{yy}^{(1)}\right] + \frac{2(1+\upsilon_1)}{E_1}\tau_{y_1x}^{(1)}\,\delta\tau_{y_1x}^{(1)}\}dxdy_1 + \int_{-L/2}^{L/2}\int_{-h_2/2}^{h_2/2}\{\frac{1}{2}\left[\sigma_{xx}^{(2)}\delta\varepsilon_{xx}^{(2)} + \delta\sigma_{xx}^{(2)}\varepsilon_{xx}^{(2)} + \sigma_{yy}^{(2)\delta}\varepsilon_{yy}^{(2)} + \delta\sigma_{yy}^{(2)}\varepsilon_{yy}^{(2)}\right] + \frac{2(1+\upsilon_2)}{E_2}\tau_{y_2x}^{(2)}\delta\tau_{y_2x}^{(2)}\}dxdy_2, \tag{3.38}$$

where δ is the mathematical variational operator with respect to either *f* or *g*. Finally, by substituting the ply stress expressions (3.20), (3.23), (3.26), (3.27), (3.30) and (3.33) as well as normal strains (3.35) and (3.36) into (3.38) and evoking the variational operations and mathematical simplifications, it turns out that *f* and *g* satisfy a set of two coupled 4th-order linear ODEs of constant coefficients as

$$[A]\{\Phi^{(IV)}\} + [B]\{\Phi''\} + [C]\{\Phi\} + \{D\} = \{0\}. \tag{3.39}$$

In the above {Φ}is defined as

$$\{\Phi\} = \{F(\xi), G(\xi)\}^T, \tag{3.40}$$

where

$$F(\xi) = F\left(\frac{x}{h_2}\right) = \frac{1}{p_1 h_2}\int_0^x f(\zeta)d\zeta, \tag{3.41a}$$

$$G(\xi) = G\left(\frac{x}{h_2}\right) = \frac{1}{p_1 h_2^2}\int_0^x\int_0^\zeta g(\eta)d\eta d\zeta. \tag{3.41b}$$

[A], [B] and [C] are 2 × 2 square symmetric coefficient matrices related to laminate geometries and [D] matrices related to the external load can be given as

$$[A] = \begin{bmatrix} \frac{2h_{12}^3}{105} + \frac{e_{12}}{30} & \frac{11h_{12}^2}{105} - \frac{e_{12}}{6} \\ \text{sys} & \frac{26h_{12}}{35} + e_{12} \end{bmatrix}, \tag{3.42a}$$

$$[B] = -\begin{bmatrix} \frac{8h_{12}}{15} + \frac{2}{3}e_{12} & \frac{2-10v_1}{5} + 2v_2e_{12} \\ \text{sys} & \frac{24h_{12}^{-1}}{5} \end{bmatrix}, \tag{3.42b}$$

$$[C] = 4\begin{bmatrix} 2h_{12}^{-1} + e_{12} & 3h_{12}^{-2} \\ \text{sys} & 6h_{12}^{-3} \end{bmatrix}. \tag{3.42c}$$

{D} and {0} are two vectors defined as

$$\{D\} = -\begin{Bmatrix} D_1 \\ 0 \end{Bmatrix}, \tag{3.42d}$$

$$\{0\} = \{0,0\}^{\mathrm{T}}. \tag{3.42e}$$

and h_{12} and $e_{12}$are respectively the ply thickness ratio and the ratio of Young's moduli of the upper and middle plies as

$$h_{12} = \frac{h_1}{h_2}, \tag{3.42f}$$

$$e_{12} = \frac{E_1}{E_2}, \tag{3.42g}$$

$$D_1 = \begin{cases} 2 + \dfrac{(\alpha_1 - \alpha_2)\Delta T E_1}{p_1} & \text{(for mechanical and thermal loads} - \text{plane stress)}, \\ 2 & \text{(for mechanical loads} - \text{plane stress)}, \\ \dfrac{(\alpha_1 - \alpha_2)\Delta T E_1}{p_1} & \text{(for thermal loads} - \text{plane stress)}. \end{cases} \tag{3.42h}$$

The solution of Eq. (3.39) can be obtained by superimposing the general solution {Ψ} of the corresponding set of homogenous ODEs onto a particular solution {Φ_0}:

$$\{\Phi\} = \{\Psi\} + \{\Phi_0\}, \tag{3.43}$$

$$[A]\{\Psi^{(IV)}\} + [B]\{\Psi''\} + [C]\{\Psi\} = \{0\}, \tag{3.44}$$

$$\{\Phi_0\} = -[C]^{-1}\{D\}. \tag{3.45}$$

To solve the system of homogenous ODEs as mentioned in (3.44), the general solution $\{\Psi\}$is assumed as:

$$\{\Psi\} = \{\Psi_0\}\, exp(\lambda\xi), \tag{3.46}$$

where λ and $\{\Psi_0\}$ represent the eigenvalue and eigenvector, respectively, of the characteristic equation associated with (3.44):

$$\lambda^4[A]\{\Psi_0\} + \lambda^2[B]\{\Psi_0\} + [C]\{\Psi_0\} = \{0\}. \tag{3.47}$$

By introducing a new variable vector

$$\{\Psi_1\} = \lambda^2\{\Psi_0\}, \tag{3.48}$$

the eigenvalue problem (3.47) can be transformed into a generalized eigenvalue problem:

$$\begin{bmatrix} I & 0 \\ 0 & A \end{bmatrix}\begin{Bmatrix} \Psi_0 \\ \Psi_1 \end{Bmatrix} = -\lambda^{-2}\begin{bmatrix} 0 & \text{-I} \\ C & B \end{bmatrix}\begin{Bmatrix} \Psi_0 \\ \Psi_1 \end{Bmatrix}. \tag{3.49}$$

By utilizing eig( ) function available in Matlab™ , eigenvalue problem (3.48),can efficiently solved. Thus, the final expression of the general solution (3.39) is

$$\{\Phi\} = \sum_{k=1}^{4}[c_k\{\Psi_0^k\}\, exp(\lambda_k\xi) + d_k\{\Psi_0^k\}\, exp(-\lambda_k\xi)] + \{\Phi_0\}, \tag{3.50}$$

where $\{\Psi_0^k\}$ (k = 1, 2, 3, and 4) are eigenvectors attached to eigenvalues λ_k (k = 1, 2, 3, and 4), respectively, and c_k and d_k (k = 1, 2, 3, and 4) are the real or complex coefficients to be determined to satisfy the traction BCs (3.8) - (3.9l). Only eight BCs are linearly independent and can be extracted from (3.8) - (3.9l) for determining c_k and d_k (k = 1, 2, 3, and 4) as

$$F[-L/(2h_2)] = 0, \tag{3.51a}$$

$$F[L/(2h_2)] = 0, \tag{3.51b}$$

$$F'[-L/(2h_2)] = 0, \tag{3.51c}$$

$$F'[L/(2h_2)] = 0, \tag{3.51d}$$

$$\mathrm{G}[-L/(2h_2)] = 0, \tag{3.51e}$$

$$\mathrm{G}[L/(2h_2)] = 0, \tag{3.51f}$$

$$\mathrm{G}'[-L/(2h_2)] = 0, \tag{3.51g}$$

$$\mathrm{G}'[L/(2h_2)] = 0. \tag{3.51h}$$

Consequently, substitution of (3.50) into (51a)-(51h) leads to a set of eight linear algebraic equations:

$$\sum_{k=1}^{4} c_k \Psi_0^{k,1}\, exp[-\lambda_k L/(2h_2)] + \sum_{k=1}^{4} d_k \Psi_0^{k,1}\, exp[\lambda_k L/(2h_2)] = -\Phi_0^{(1)}, \tag{3.52a}$$

$$\sum_{k=1}^{4} c_k \Psi_0^{k,1}\, exp[\lambda_k L/(2h_2)] + \sum_{k=1}^{4} d_k \Psi_0^{k,1}\, exp[-\lambda_k L/(2h_2)] = -\Phi_0^{(1)}, \tag{3.52b}$$

$$\sum_{k=1}^{4} c_k \lambda_k \Psi_0^{k,1}\, exp[-\lambda_k L/(2h_2)] - \sum_{k=1}^{4} d_k \lambda_k \Psi_0^{k,1}\, exp[\lambda_k L/(2h_2)] = 0, \tag{3.52c}$$

$$\sum_{k=1}^{4} c_k \lambda_k \Psi_0^{k,1}\, exp[\lambda_k L/(2h_2)] - \sum_{k=1}^{4} d_k \lambda_k \Psi_0^{k,1}\, exp[-\lambda_k L/(2h_2)] = 0, \tag{3.52d}$$

$$\sum_{k=1}^{4} c_k \Psi_0^{k,2}\, exp[-\lambda_k L/(2h_2)] + \sum_{k=1}^{4} d_k \Psi_0^{k,2}\, exp[\lambda_k L/(2h_2)] = -\Phi_0^{(2)}, \tag{3.52e}$$

$$\sum_{k=1}^{4} c_k \Psi_0^{k,2}\, exp[\lambda_k L/(2h_2)] + \sum_{k=1}^{4} d_k \Psi_0^{k,2}\, exp[-\lambda_k L/(2h_2)] = -\Phi_0^{(2)}, \tag{3.52f}$$

$$\sum_{k=1}^{4} c_k \lambda_k \Psi_0^{k,2}\, exp[-\lambda_k L/(2h_2)] - \sum_{k=1}^{4} d_k \lambda_k \Psi_0^{k,2}\, exp[\lambda_k L/(2h_2)] = 0, \tag{3.52g}$$

$$\sum_{k=1}^{4} c_k \lambda_k \Psi_0^{k,2}\, exp[\lambda_k L/(2h_2)] - \sum_{k=1}^{4} d_k \lambda_k \Psi_0^{k,2}\, exp[-\lambda_k L/(2h_2)] = 0, \tag{3.52h}$$

In the above, $\Psi_0^{k,1}$ and $\Psi_0^{k,2}$ (k = 1, 2, 3, and 4) are respectively the 1st and 2nd elements of the k-th eigenvector, and $\Phi_0^{(1)}$and $\Phi_0^{(2)}$ are the 1st and 2nd elements of $\{\Phi_0\}$. Moreover, for thermomechanical stress analysis of the composite laminate due to a pure temperature change, the right terms of (3.9a) and (3.9b) should be zeros since p_1, which does not influence the right terms in BCs of (3.51). Therefore, once c_k and d_k (k = 1, 2, 3, and 4) are determined by solving the above system of linear algebraic equations (3.52a) - (3.52h) numerically, expressions (3.41a), (3.41b) and (3.50) give the final expression of f and g as

$$\frac{f(x)}{p_1} = \sum_{k=1}^{4} c_k \Psi_0^{k,1} \lambda_k \, exp(-\lambda_k x/h_2) - \sum_{k=1}^{4} d_k \Psi_0^{k,1} \lambda_k \, exp(\lambda_k x/h_2), \tag{3.53a}$$

$$\frac{g(x)}{p_1} = \sum_{k=1}^{4} c_k \Psi_0^{k,2} \lambda_k^2 \, exp(-\lambda_k x/h_2) + \sum_{k=1}^{4} d_k \Psi_0^{k,2} \lambda_k^2 \, exp(\lambda_k x/h_2). \tag{3.53b}$$

Consequently, with f and g given in (3.53a) and (3.53b), all the planar stress components in the composite laminate can be determined using the stress expressions formulated in Section 3.1.3.

Furthermore, the strain energy of the composite laminate system per unit longitudinal length can be expressed as

$$\begin{aligned} e = 2 \int_{-h_1/2}^{h_1/2} \{ \frac{1}{2} [\sigma_{xx}^{(1)} \varepsilon_{xx}^{(1)} + \sigma_{yy}^{(1)} \varepsilon_{yy}^{(1)}] + \frac{v_1(1+v_1)}{E_1} [\tau_{xy_1}^{(1)}]^2 \} dy_1 \\ + \int_{-h_2/2}^{h_2/2} \{ \frac{1}{2} [\sigma_{xx}^{(2)} \varepsilon_{xx}^{(2)} + \sigma_{yy}^{(2)} \varepsilon_{yy}^{(2)}] + \frac{v_2(1+v_2)}{E_2} [\tau_{xy_2}^{(2)}]^2 \} dy_2. \end{aligned} \tag{3.54}$$

The strain energy density (3.54) can be expressed utilizing the governing ODE (3.39),

$$e = \frac{1}{2} \{\Phi\}^T \{D\} \frac{p_1^2 h_2}{E_1} + \frac{h_1}{E_1} p_1^2. \tag{3.55}$$

Substitution of (3.50) into (3.55) leads to

$$e(\xi) = \frac{1}{2}\sum_{k=1}^{4}[c_k\{\Psi_0^k\}^T\{D\}\,exp(\,\lambda_k\xi) + d_k\{\Psi_0^k\}^T\{D\}exp(-\lambda_k\xi)]\frac{p_1^2h_2}{E_2} - \frac{1}{2}\{D\}^T\{C\}^{-1}\{D\}\frac{p_1^2h_2}{E_1} + \frac{h_1}{E_1}p_1^2. \tag{3.56}$$

In Eq. (3.56), the first term represents the additional strain energy stored in the material due to the presence of localized stress concentration caused by cracking (specifically, two free ends). This term is dependent on the geometric properties and elastic characteristics of the laminate. The remaining part of the equation represents the strain energy density of the laminate without any cracks, denoted as e_0, i.e.,

$$e_0 = -\frac{1}{2}\{D\}^T\{C\}^{-1}\{D\}\frac{p_1^2h_2}{E_1} + \frac{h_1}{E_1}p_1^2. \tag{3.57}$$

Furthermore, the strain energy density associated with the laminate with a single crack in the middle ply (left-half $\xi > 0$) is

$$e_\infty(\xi) = \frac{1}{2}[d_k\{\Psi_0^k\}^T\{D\}\,exp(-\lambda_k\xi)]\frac{p_1^2h_2}{E_2} - \frac{1}{2}\{D\}^T\{C\}^{-1}\{D\}\frac{p_1^2h_2}{E_1} + \frac{h_1}{E_1}p_1^2, \tag{3.58}$$

where λ_k (k =1, 2, 3 and 4) are the four eigenvalues with positive real parts, d_k (k = 1, 2, 3, and 4) are determined to satisfy the traction BCs, which leads to a system of four linear algebraic equations:

$$\sum_{k=1}^{4} d_k\Psi_0^{k,1}\,exp[\,\lambda_kL/(2h_2)] = -\Phi_0^{(1)}, \tag{3.59a}$$

$$\sum_{k=1}^{4} d_k\lambda_k\Psi_0^{k,1}\,exp[\,\lambda_kL/(2h_2)] = 0, \tag{3.59b}$$

$$\sum_{k=1}^{4} d_k\Psi_0^{k,2}\,exp[\,\lambda_kL/(2h_2)] = -\Phi_0^{(2)}, \tag{3.59c}$$

$$\sum_{k=1}^{4} d_k \lambda_k \Psi_0^{k,2} \, exp[\, \lambda_k L/(2h_2)] = 0. \tag{3.59d}$$

3.1.5. Progressive cracking analysis

Within the framework of LEFM, criterion of through thickness cracking in the mid-ply of the composite laminate subjected to a tensile stress, denoted as p_1, is that the strain energy increase ΔU due to cracking is equal to the strain energy release $\Delta\Gamma$ [45-46]:

$$\Delta U = \Delta\Gamma = G_c h_2, \tag{3.60}$$

where G_c is the critical strain energy release rate (ERR) or fracture toughness of the mid-ply. Therefore, it is only necessary to examine the strain energy variation before and after the occurrence of through-thickness cracking within the mid-ply.

The cracking threshold (3.60) for the initiation of the first cracking can be determined by utilizing strain energy densities (3.57) and (3.58) as

$$G_c h_2 = 2 \int_0^{+\infty} [e_\infty(\xi) - e_0] d\xi, \tag{3.61}$$

which can be reduced as

$$\sum_{k=1}^{4} d_k \lambda_k^{-1} \{\Psi_0^k\}^T \{D\} \frac{p_1^2 {h_2}^2}{E_1} = G_c h_2. \tag{3.62}$$

Expression (3.62) contains a quadratic term involving variable p_1 on its left side. Furthermore, the right term of Eq. (3.62) can be rewritten as

$$\sum_{k=1}^{4} d_k \lambda_k^{-1} \{\Psi_0^k\}^T \{D\} \frac{p_1^2 h_2}{E_1} = A_{pp} p_1^2, \tag{3.63}$$

where A_{pp} is the coefficient relating the geometries and material properties of the laminate. Eq. (3.63) represents the general strain energy criterion governing the initiation of first cracking in the mid-ply.

3.1.5.1. Progressive cracking and crack spacing in the mid-ply

In order to examine the progressive cracking in the mid-ply of the present composite laminate, it is crucial to determine the correlation of the crack density to the external loads. When the laminate is subjected to a uniaxial tensile force with a gradually increasing magnitude. progressive cracking happens once the force magnitude reaches the threshold related to the specific crack density. This indicates that a newborn cracking happens between two consecutive cracks with a given spacing L in the laminate when the uniaxial tensile force reaches the threshold related to L (see Figure 3.2). Hence, it is rational to first examine the incidence of the subsequent cracking at a random site C located between loci A and B.

According to the strain energy criterion (3.60) for cracking, it leads to

$$G_c h_2 = \int_0^{s_1} e(\xi) d\xi + \int_0^{s_2} e(\xi) d\xi - \int_0^{s} e(\xi) d\xi, \tag{3.64}$$

where $s_1 = L_1/h_2$, $s_2 = L_2/h_2$, $s = L/h_2 = (s_1 + s_2)$ and $e(\xi)$ is given by (3.56). The three integrals in (3.64) can be expressed explicitly:

$$G_c h_2 = \Pi_1 + \Pi_2 - \Pi_3, \tag{3.65}$$

where

$$\Pi_1 = \left\{\sum_{k=1}^{4} sinh\frac{\lambda_k s_1}{2}\left[c_k\lambda_k^{-1}\exp(\frac{\lambda_k s_1}{2})\{\Psi_0^k\}^T + d_k\lambda_k^{-1}\exp(\frac{-\lambda_k s_1}{2})\{\Psi_0^k\}^T\right]\right\}\{D\}\frac{p_1^2 {h_2}^2}{E_1}, \tag{3.66a}$$

$$\Pi_2 = \left\{\sum_{k=1}^{4} sinh\frac{\lambda_k s_2}{2}\left[c_k\lambda_k^{-1}\exp(\frac{\lambda_k s_2}{2})\{\Psi_0^k\}^T + d_k\lambda_k^{-1}\exp(\frac{-\lambda_k s_2}{2})\{\Psi_0^k\}^T\right]\right\}\{D\}\frac{p_1^2 {h_2}^2}{E_1}, \tag{3.66b}$$

$$\Pi_3 = \left\{\sum_{k=1}^{4} sinh\frac{\lambda_k s_3}{2}\left[c_k\lambda_k^{-1}\exp(\frac{\lambda_k s_3}{2})\{\Psi_0^k\}^T + d_k\lambda_k^{-1}\exp(\frac{-\lambda_k s_3}{2})\{\Psi_0^k\}^T\right]\right\}\{D\}\frac{p_1^2 {h_2}^2}{E_1}. \tag{3.66c}$$

In the above, coefficients c_k and d_k (k = 1, 2, 3, and 4) in (3.66a-c) are the same as given in (3.50) with $\frac{L}{h_2} = s_1$, s_2 and s, respectively.

The critical loads are determined by relation (3.65) for either a specified single load or combined loads with a constant ratio. Without loss of generality, position C of the newborn cracking can be considered as a stochastic variable. Therefore, it is beneficial to employ a probability density function p to describe the random position of the subsequent cracking. The expected value of the external threshold load P_c (for tensile traction p_1) to induce the next cracking in the mid-ply which already contains cracks with the crack density d (=1/L) is

$$E[P_c(s)] = h_2\int_0^s p(\xi)p_c(\xi)d\xi. \tag{3.67}$$

Selection of the probability density function is vital in determining the mean threshold load $E[P_c(s)]$ [11].

3.2. Numerical Solutions and Validation

3.2.1. Interfacial stresses due to mechanical loads

To validate the analytical model developed in the previous section, a commercial FEA software package (ANSYS Mechanical APDL^{TM}) is used to determine the interfacial shear and normal stresses in a three-layered cross-ply composite laminate subjected to uniaxial tension. Due to the symmetries of the laminate geometries and material properties as well as the applied loads, the interfacial shear and normal stresses at the upper and lower interfaces of the laminate are identical. The geometrical parameters of the three-layered cross-ply composite laminate (Graphite/epoxy: T300/934) taken in FEA are L = 20 mm, h_1 = 2.00 mm (upper layer where the fiber direction is along with the uniaxial tensile loads), and h_2= 4.00 mm (mid-layer where the fiber direction is transverse to the loads). For the convenience of comparison, each ply of the laminate is assumed as an isotropic, linearly elastic solid. The elastic properties of the upper ply are given as the Young's modulus of E_1 = 138 GPa and Poisson's ratio of ν_1= 0.29, The elastic properties of the mid-ply are given as the Young's modulus of E_2 = 11.7 GPa and Poisson's ratio of ν_2 = 0.4 The magnitude of the uniform tensile stress p_1 is assumed to be 1.0 MPa.

The FEM-based stress analysis (ANSYS^{TM}) of this three-layered symmetric cross-ply laminate utilizes four-node elements (PLANE182) and mapped uniform quadrilateral meshes. To approach the varying trend of the singular stresses at the free edge, three different mesh sizes (i.e., 0.05 × 0.05 mm, 0.1 × 0.1 mm, and 0.2 × 0.2 mm) are used in FEA. Figure 3.5 shows the meshed symmetric right-top quarter of the cross-ply laminate as used in the linear FEA. Figures 3.6 (a) and (b) show the variations of the interfacial shear and normal stresses of the cross-ply composite laminate as predicted by the present stress-functional variational method which are compared with the computational results generated by ANSYS^{TM}. It can be found that the

present analytical model is capable of accurately predicting the variations of the interfacial shear and normal stresses along the ply interfaces of this cross-ply composite laminate.

During the process, a constant traction of 1.0 MPa is employed as the axial load. The mismatch of the mechanical properties of neighboring plies leads to the high interfacial stress concentrations near the free edges. Such high singular interfacial stresses are responsible for the interlaminar delamination near the laminate free edges, one of the main concerns in the design and analysis of composite structures.

Figure 3.5 The symmetric top-right quarter portion of the three-layered laminate segment used in FEA based on ANSYS ™.

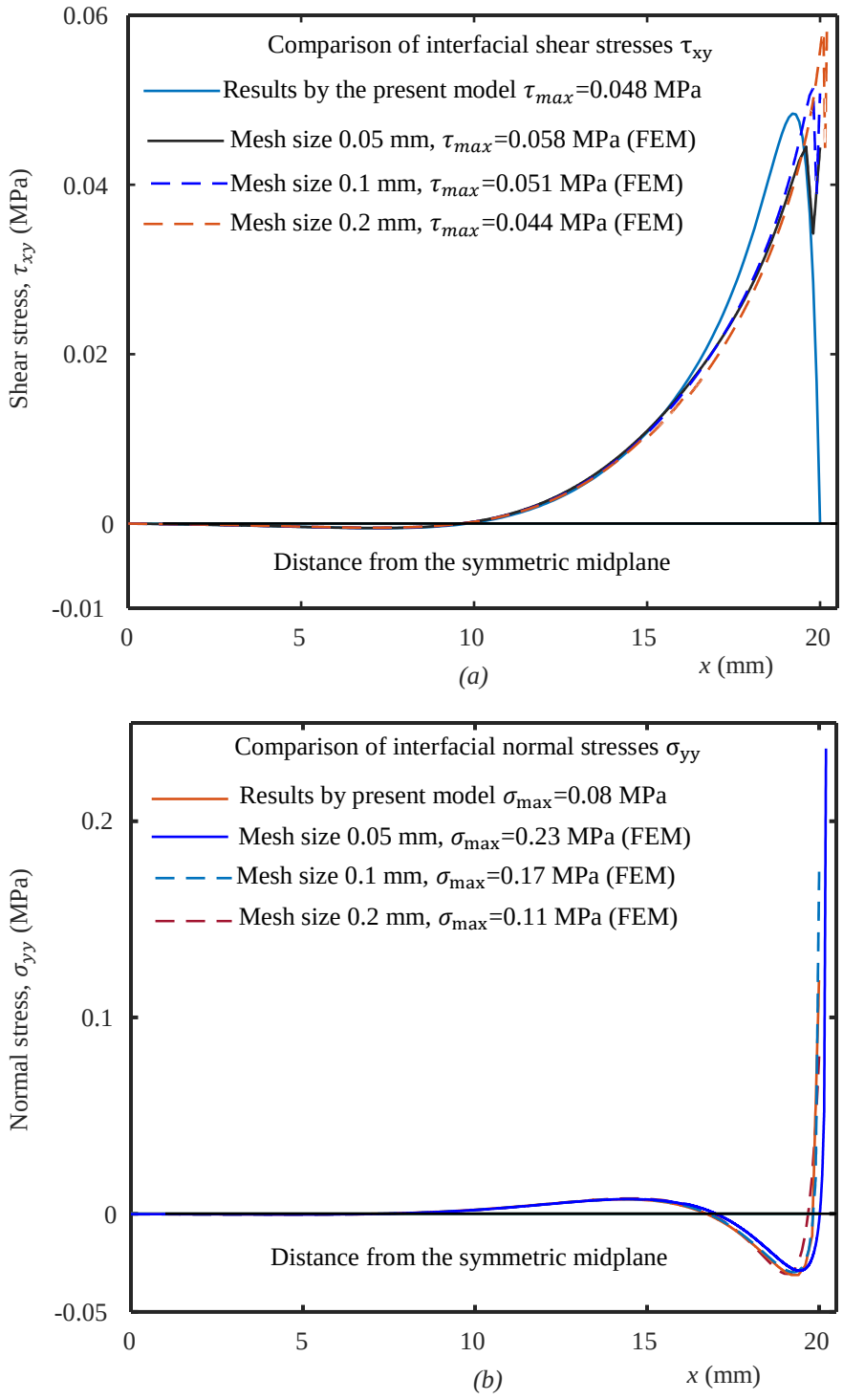

Figure 3.6 Comparisons of the interfacial shear and normal stresses predicted by the present semi-analytical model with those calculated by FEM (ANSYS^{TM}): (a) The interfacial shear stress and (b) The interfacial normal stress.

3.2.2. Scaling analysis of interfacial stresses due to mechanical loads

This section is to analyze the relationship between interfacial stresses and the geometries and material characteristics of the three-layered composite laminate. Specifically, the impact of the length ratio L/h_2, thickness ratio h_1/h_2, and modulus ratio E_1/E_2 on these interfacial stresses are examined in details. To conduct such scaling analysis, four thickness ratios (h_1/h_2 = 0.5, 1.0, 1.5, & 2.0), two length ratios (L/h_2= 5 & 10), and two modulus ratios (E_1/E_2 = 10 & 15) are adopted, respectively. A concise and efficient computational program has been designed to implement the current stress-function variational method for analyzing the interfacial stresses in this three-layered cross-ply composite laminate under consideration. This program can be utilized to explore the relationship between interfacial shear and normal stresses and various geometrical and material properties. During the scaling analysis, the two Poisson's ratios, i.e., ν_1= 0.29 and ν_2= 0.40 of the upper and middle plies, respectively, are fixed and plane-stress state is assumed.

Figures 3.7-3.10 show the variations of the dimensionless interfacial shear stress τ/p_1 and normal stress σ/p_1 at the interfaces with the dimensionless distance x/h_2 from the symmetric midspan of the uncracked laminate segment to the right crack surface.

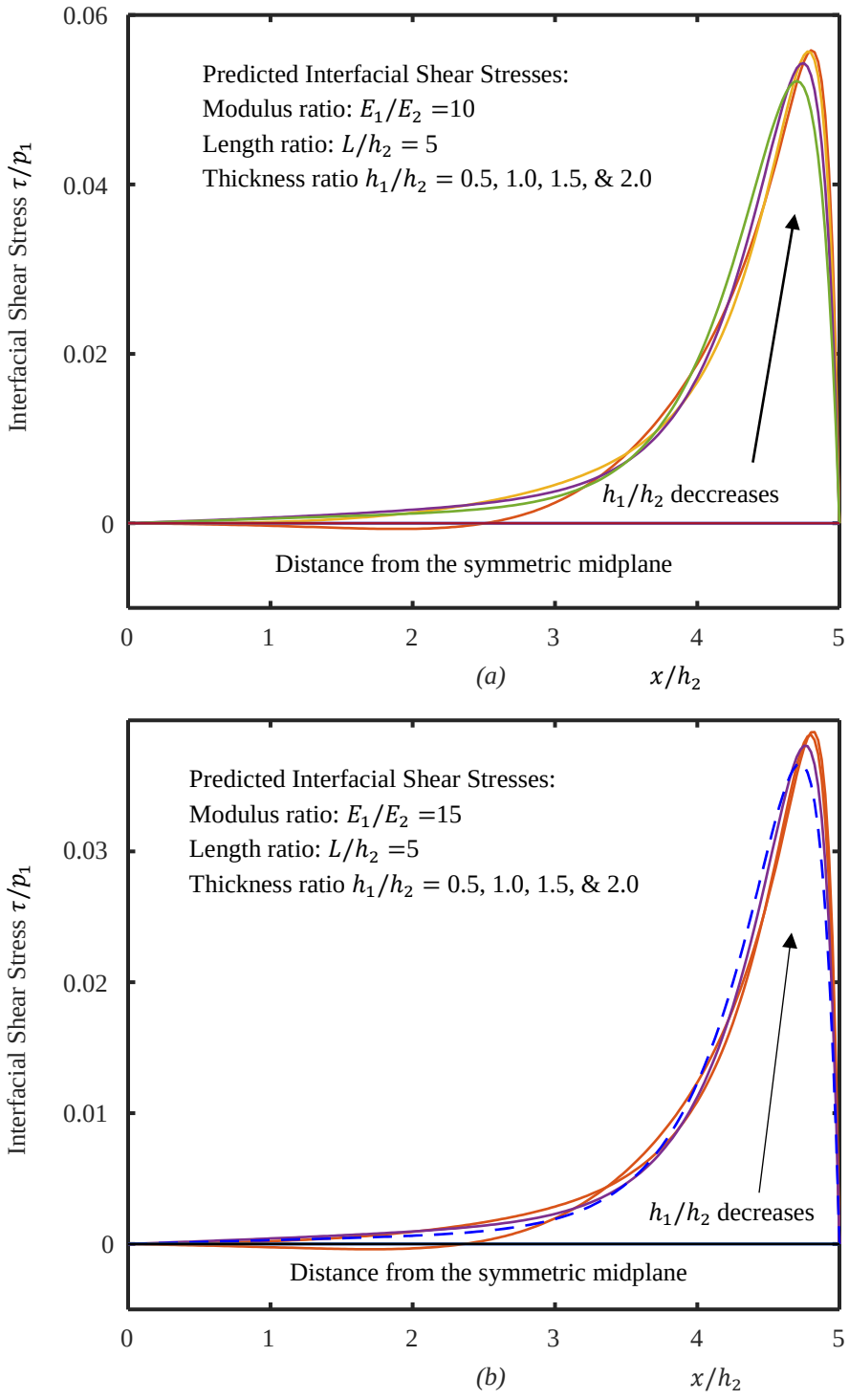

Figure 3.7 Comparison of the variations of the dimensionless interfacial shear stresses in the cross-ply laminate over the dimensionless distance from the symmetric midspan: (*a*) The shear stress for the length ratio L/h_2= 5 and modulus ratio E_1/E_2 =10, (*b*) The shear stress for the length ratio L/h_2= 5 and modulus ratio E_1/E_2 = 15

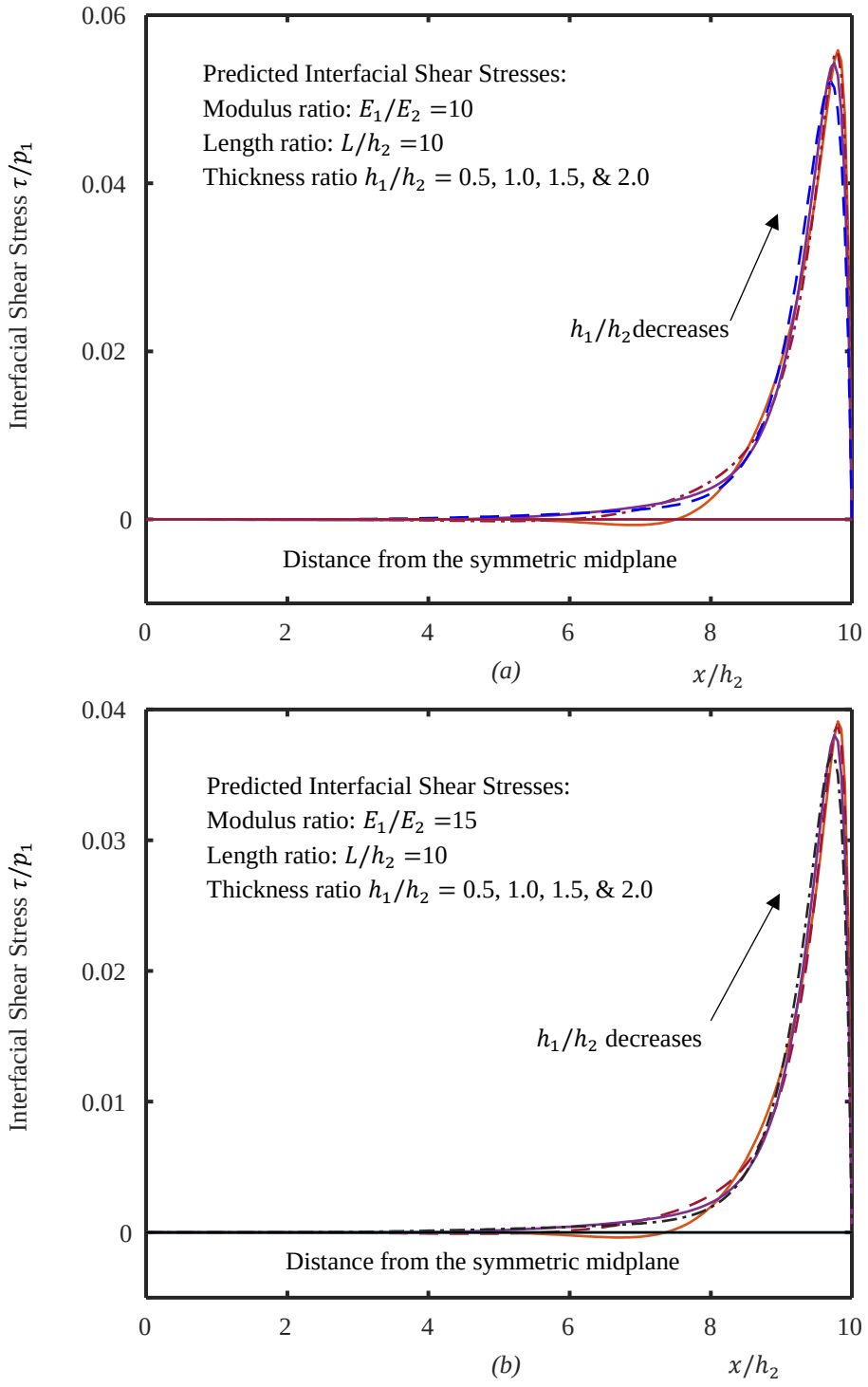

Figure 3.8 Comparison of the variations of the dimensionless interfacial shear stresses in the cross-ply laminate over the dimensionless distance from the symmetric midspan: (a) The shear stress for the length ratio L/h_2=10 and modulus ratio E_1/E_2 =10, (b) The shear stress for the length ratio L/h_2= 10 and modulus ratio E_1/E_2 = 15.

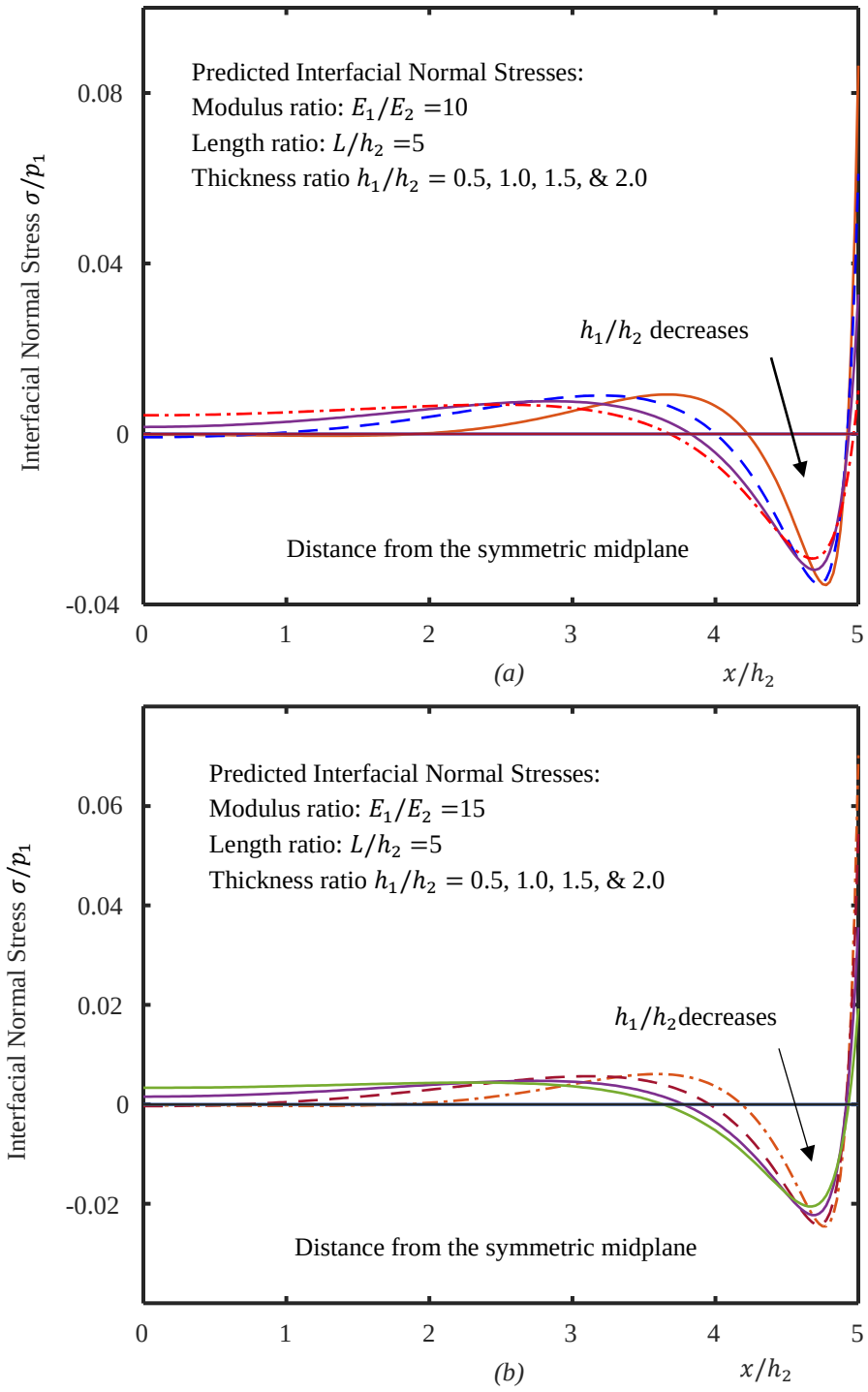

Figure 3.9 Comparison of the variations of the dimensionless interfacial normal stresses in the cross-ply laminate over the dimensionless distance from the symmetric midspan: *(a)* The normal stress for the length ratio L/h_2 = 5 and modulus ratio E_1/E_2 = 10, *(b)* The normal stress for the length ratio L/h_2= 5 and modulus ratio E_1/E_2 = 15.

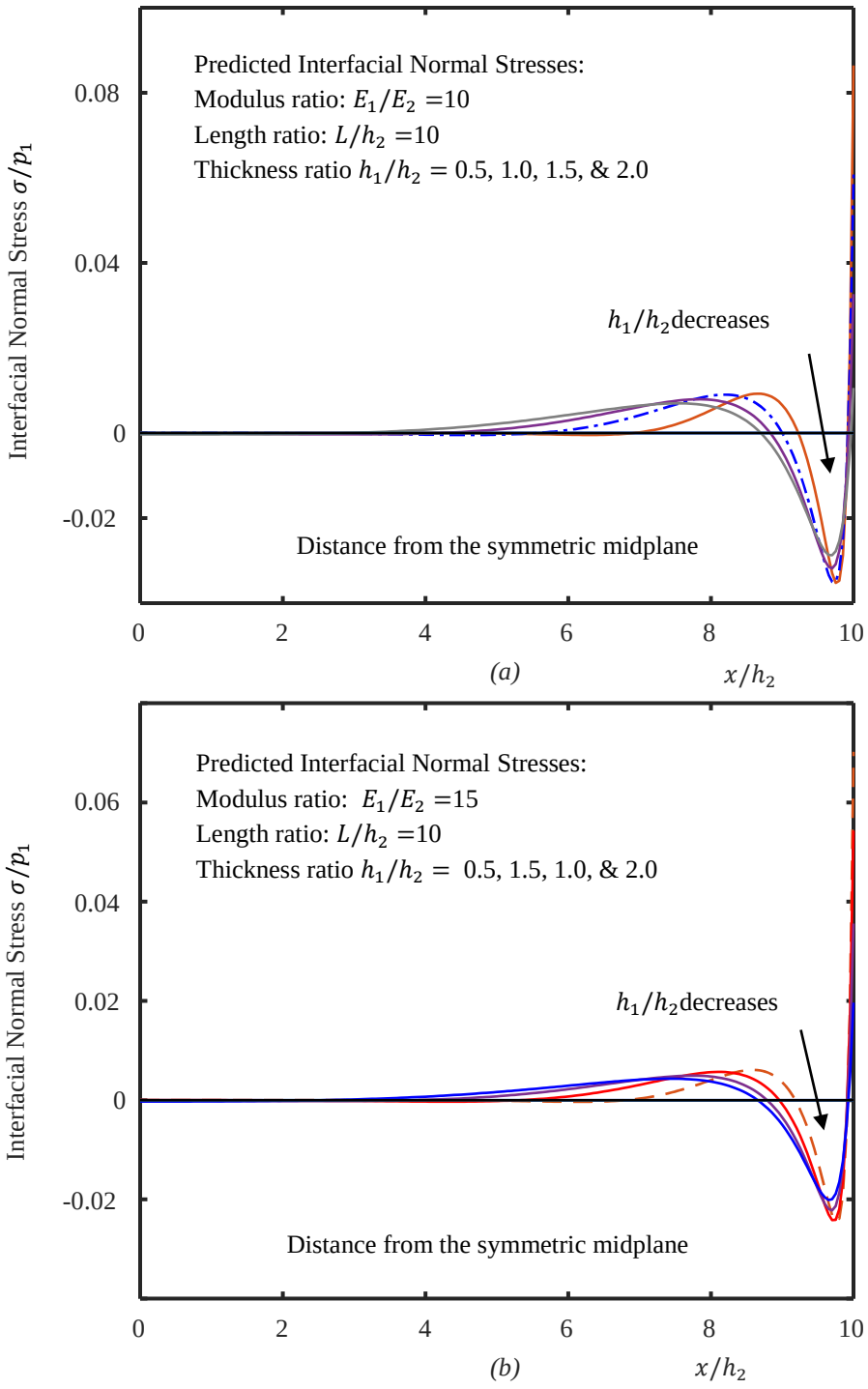

Figure 3.10 Comparison of the variations of the dimensionless interfacial normal stresses in the cross-ply laminate over the dimensionless distance from the symmetric midspan: (a) The normal stress for the length ratio L/h_2 = 10 and modulus ratio E_1/E_2 = 10, (b) The normal stress for the length ratio L/h_2 = 10 and modulus ratio E_1/E_2 = 15.

From the above scaling analysis, the present semi-analytic model predicts the high interfacial stress concentration at the free edges of the three-layered cross-ply laminates. In each study case, the interfacial normal stress significantly exceeds the interfacial shear stress at the free edges. Moreover, in all the case, the predicted interfacial shear stresses at the free edges of the laminate approach zero, which fulfills the shear-free BC at the free edges.

Regarding the interfacial shear stresses, when the thickness ratio (h_1/h_2) increases, the peak value of the interfacial share stress decrease. Similar stress variations are also observed for interfacial normal stresses. The peak normal stress increases with decreasing thickness ratio (h_1/h_2). Additionally, the above stress diagrams also indicate that, the length ratio L/h_2, i.e., the ratio of the length of laminate to the thickness of mid-ply, does not affect the interfacial stresses noticeably. Given a fixed length ratio L/h_2, a higher flexural rigidity of the laminate due to the higher modulus ratio E_1/E_2, i.e., the higher modulus in the longitudinal direction included by the stiff reinforcing fibers, or the higher thickness ratio h_1/h_2, i.e., the thicker upper-ply, leads to a lower stress concentration of both the interfacial shear and normal stresses at the free edges of this composite laminate.

3.2.3. Crack density in the mid-ply

This section is to examine the progressive cracking process in the three-layered symmetric cross-ply composite laminate. For a gradually increasing uniaxial tensile load, the first cracking arises in the mid-ply upon meeting criterion (Eq. 3.61). Once the initial cracking occurs, progressive cracking begins to evolve with the escalating loads according to relation (Eq. 3.65). In this analysis, the focus is on the change in the dimensionless crack spacing with the

dimensionless critical load $p_1 h_2/G_{IC}$, more precisely, in the case of uniaxial stress prior to formation of a single crack as explored in the preceding section.

The critical load is defined as the predicted value at which the next crack is expected to occur, provided it is equidistant from the existing cracks, with a spacing of L/h_2, as outlined in Eq. (3.64) with $L_1 = L_2$. Figure 3.11 shows the correlation between the dimensionless crack spacing and the dimensionless critical load at four thickness ratios ($h_1/h_2 = 0.5, 1.0, 1.5,$ & 2.0) and two modulus ratios ($E_1/E_2 = 10, 20$). The numerical results shown that given a crack spacing, a decrease in the thickness of the upper ply or an increase in the thickness of the mid-ply results in reduced threshold load. Conversely, in the case of stiffer upper and lower plies, a higher threshold load is necessitated, or on the other hand, a flexible mid-ply expects a higher threshold load. This relationship indicates that an increase in the E_1/E_2 ratio facilitates enhanced crack resistance, compared to scenarios where the ratio is comparatively lower.

The above numerical test results are in align with the previously predicted interfacial stress patterns. A thicker and more rigid mid-ply not only results in elevated interfacial shear and normal stresses, typically associated with delamination failure, but it also demonstrates reduced resistance to crack initiation and growth within the mid-ply. This phenomenon can be understood in the sense of the principle of energy conservation, wherein highly stressed, stiffened, and thick mid-ply possesses the capability to release an adequate amount of strain energy, thereby promoting the spontaneous crack initiation and growth.

This observation is compatible with the findings reported in the literature [15], wherein the progressive cracking of a hard surface coating was predicted. The current model demonstrates a noteworthy agreement with that study. Notably, in the progressive cracking analysis in a hard surface coating [15], the authors employed the same stress function variational

technique. Within the scope of this study, it is observed that as the coating surface-to-substrate layer thickness ratio or modulus ratio decreases, the threshold load for to initiate cracking also experiences an increase, mirroring the trends as observed in the present model. It is imperative to highlight that the disparity between the two models lies in the location of crack initiation. In the present study, cracking occurs in the mid-ply, while cracking manifests in the upper surface coating layer in the referenced study.

This section substantiates the ongoing progressive cracking model by examining experimental data retrieved from the existing literature. Highsmith et al. [54] conducted the experiments on an E-glass-epoxy cross-ply composite laminate$(0,90)_s$. The authors specified the material properties as follows: E_1 = 41.7 GPa (in the longitudinal fiber direction), ν_1= 0.3 (in the in-plane Poisson's ratio), E_2 = 13 GPa (in the transverse direction), and ν_2 = 0.45 (the out-of-plane Poisson's ratio). Although the paper does not provide the critical energy release rate G_c values, the same experimental data, as referenced by [26,31,55], utilizes a $G_c$value of 193 Jm^{-2}. Figure 3.12 shows the effect of the applied load (MPa) on the crack density (cracks/cm). The present model, as depicted in Figure 3.12, demonstrates a good agreement with the experimental data. Consequently, it is noteworthy that an increase in the thickness ratio, as discussed earlier, reduces the crack density for the same applied load, particularly accentuating the phenomenon observed in the thin mid-plies.

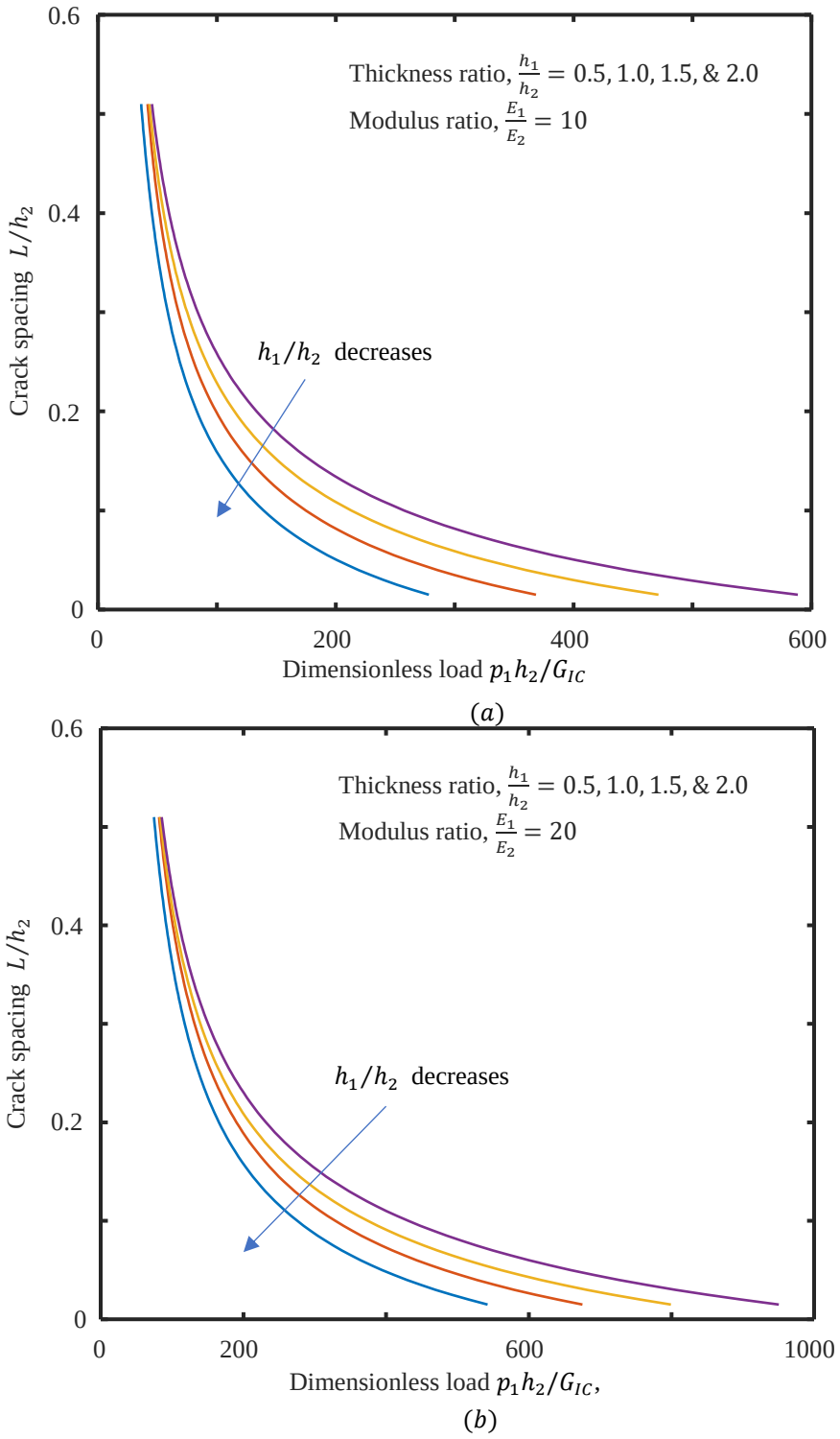

Figure 3.11 Variations of the dimensionless crack spacing vs the dimensionless critical load at thickness ratio of $\frac{h_1}{h_2} = 0.5, 1.0, 1.5, \& 2.0$ at (a) Modulus ratio of $\frac{E_1}{E_2} = 10$ (b) Modulus ratio of $\frac{E_1}{E_2} = 20$, respectively.

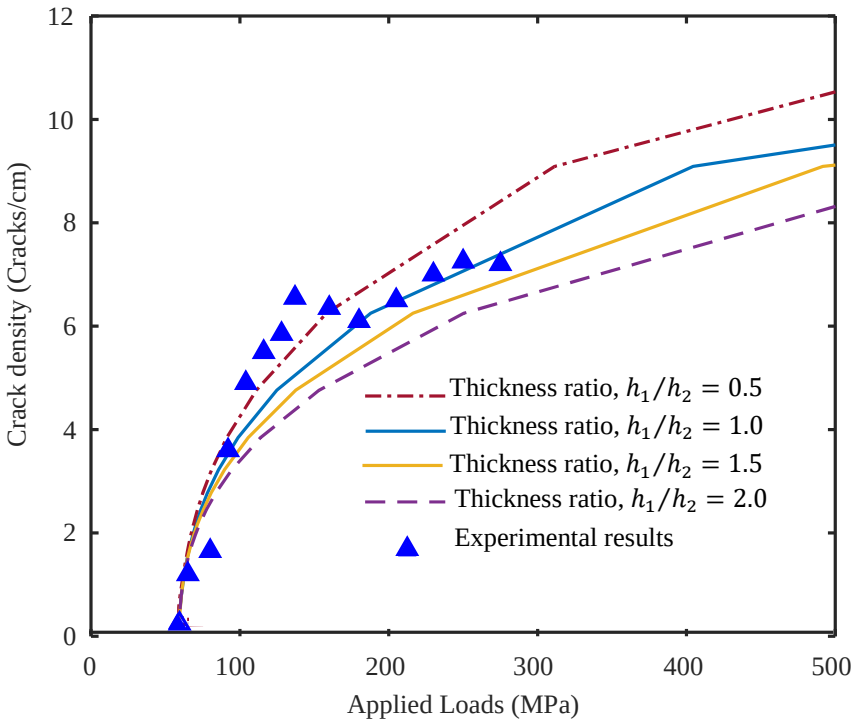

Figure 3.12 Comparison of the progressive cracking in E-glass-epoxy composite laminates by present model with different thickness ratios and experimental data from [54]

4. INTERFACIAL THERMOSTRESSES IN BONDED CIRCULAR BIMATERIAL THERMOSATS

4.1. Introduction

It is common that electronic devices are composite constructions or multilateral devices made from layered dissimilar materials. The performance of an electronic device is largely dependent on its design and construction. The device energy dissipation, thermal durability, and the amount of mechanical interference and vibration that a device can tolerate without loss of functionality are all influenced by the microelectronic design and construction. Electronic devices are typically joined by adhesive or solder [47]. However, contemporary microelectronics devices behave mechanically more flexible in nature, and solder is not suitable for bonding since it is susceptible to mechanical bending and vibrations. On the other hand, adhesive is compliant, low cost, and easy to process. Which technique is used, the main consideration is that the joint or bonded materials can survive the mechanical and thermal stresses and operate smoothly without performance degradation. Much research has been carried out in this field to find the optimum design for a specific application.

This chapter is to consider the interfacial stresses in bonded circular bimaterial thermostats due to the mismatch of their elastic properties and coefficients of thermal expansions. When temperature varies, thermal stresses, strains, and displacements will be induced in the bonded materials due to their heterogeneous material properties. This will not only lead to the mechanical failure but also to the functional failure of the bonded materials. For example, if the semiconductor chip is unable to dissipate the heat properly instantaneously, high thermal stress will be accumulated, which can lead to the functionality loss of the chip. A significant number of analytical models are available in the literature. Yet, few models are based

on FEM to find the interfacial shear stress and normal stress or peeling stress, which are responsible for debonding failure of the joint [47-50].

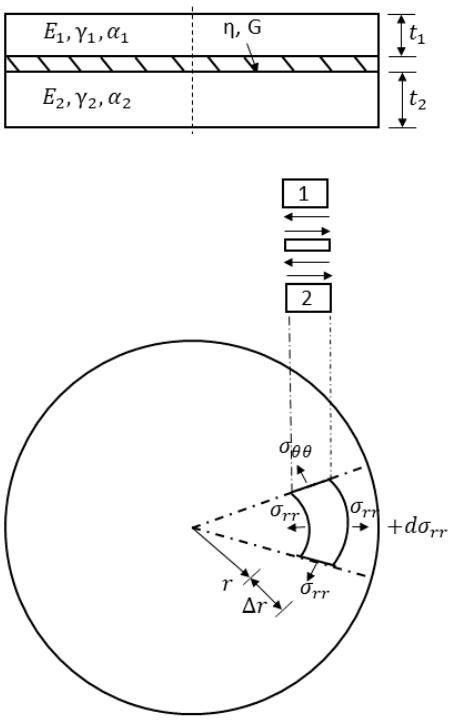

Figure 4.1 Two circular sheets bonded through an adhesive layer [Reproduced from [47]].

Consider the simplest case of two adhesively bonded circular dissimilar materials as shown in Figure 4.1. This particular case was considered earlier by Chen and Nelson in IBM [47], who developed analytical solutions using modified Bessel functions. The present model assumes an axisymmetric nature. Chen and Nelson assumed that when the bonded region is filled with adhesive, the interfacial shear stress is zero at the center and gradually increases toward the free edges. Consequently, an increase in radius corresponds to an increase in the interfacial shear stress.

Chen and Nelson concluded an analytic expression to determine the interfacial shear stress,

$$\tau = \frac{2(\alpha_1 - \alpha_2)TG}{\eta\beta(C_1 + C_2)} I_1(\beta r), \tag{4.1}$$

where C_1 and C_2 are two integration constants, and $I_1(\beta r)$ is the modified first-order Bessel functions of the first kind. In expression (4.1), Chen and Nelson defined the following parameters:

$$\beta^2 = \frac{G}{\eta}\left(\frac{1-\gamma_1^2}{E_1 t_1} + \frac{1-\gamma_2^2}{E_2 t_2}\right), \tag{4.2}$$

$$C_1 = -\frac{2}{1+\gamma_1}\left[\frac{1-\gamma_1}{\beta R} I_1(\beta r) - I_0(\beta r)\right], \tag{4.3}$$

$$C_2 = -\frac{2}{1+\gamma_2}\left[\frac{1-\gamma_2}{\beta R} I_1(\beta r) - I_0(\beta r)\right], \tag{4.4}$$

where $I_0(\beta r)$ is the modified zero-order Bessel functions of the first kind. Consequently, Chen and Nelson extracted the maximum shear stress at the end of the adherends at $r=R$ as

$$\tau_{max} = \frac{2(\alpha_1 - \alpha_2)TG}{\eta\beta(C_1 + C_2)}\left\{\frac{1}{1+\gamma_1}\left[\frac{1-\gamma_1}{\beta R} - \frac{I_1(\beta r)}{I_0(\beta r)}\right] + \frac{1}{1+\gamma_2}\left[\frac{1-\gamma_2}{\beta R} - \frac{I_1(\beta r)}{I_0(\beta r)}\right]\right\}. \tag{4.5}$$

Furthermore, Suhir et al. [49] also achieved an analytical solution similar to the one by Chen and Nelson by using modified Bessel functions. In contrast to Chen and Nelson's work [47], Suhir et al. formulated the analytic solutions for identical circular adherends, in which they treated the adherends as circular plates with small deflections, with the assumption of no effect of the interfacial normal stress on the interfacial shear stress. The maximum shear stress occurs at $r=a$ (at the end of assembly) as

$$\tau_{max} = \frac{(1+\nu_1)aI_1(ka)}{kaI_0(ka) - (1-\nu_1)I_1(ka)}\frac{\Delta\alpha\Delta t}{\kappa}, \tag{4.6}$$

where κ is the interfacial compliance of the assembly. The interfacial normal stress is expressed as

$$p_0(r) = p_{max} \frac{kaI_0\,(ka) - a\,\frac{I_1(kr)}{r}}{kaI_0\,(ka) - I_1(ka)}, \tag{4.7}$$

and p_{max} is

$$p_{max} = \frac{3}{4}\frac{1+\nu_1}{1+\nu_0}\frac{h_1}{h_0}E_0\,\frac{kaI_0\,(ka) - I_1(ka)}{kaI_0\,(ka) - (1-\nu_1)I_1(ka)}\Delta\alpha\Delta t. \tag{4.8}$$

Both of the aforementioned works provided the numerical solution. However, their analytical solutions were not well validated by FEA. The subsequent section of this chapter is to conduct FEA to determine the interfacial shear stress and normal stress resulting from thermal loading (changes in temperature) in a bonded circular bimaterial thermostat.

4.2. Finite Element Analysis of Bonded Circular Bimaterial Thermostats

A commercial FEA software package (ANSYS^{TM}) is used to analyze the aforementioned case of bonded circular bimaterial thermostats. Material properties of the two bonded circular materials are tabulated in Table 4.1. During the FEM-based computational simulation (ANSYS^{TM}), 2D axisymmetric state, four node elements (PLANE182), and uniform quadrilateral meshes are used. The reference temperature without thermal stresses is assumed as 25 °C and a temperature rise to 125 °C is considered in this modeling study. Mesh refinement is employed at the interface and near the free edge where stress concentration exists.

Figure 4.2 shows the interfacial shear stress and normal stress along the joint interface, corresponding to the numerical solutions by Chen and Nelson [47]. The maximum shear stress as identified through FEA is 28.96 MPa, in contrast to 40 MPa as reported by Chen and Nelson.

Similarly, the maximum normal stress is determined as 19 MPa, while Chen and Nelson found it to be 12.5 MPa. These disparities can be attributed to the simplification of the analytic model.

Table 4.1 Material properties of the bonded material couple

Component	Top adherend	Bottom adherend	Adhesive
Young's modulus (GPa)	117	275	3.45
Poisson ratio	0.25	0.3	0.45
Coefficient of thermal expansion $(/°C)$	1.6×10^{-5}	6.5×10^{-6}	233×10^{-6}
Thickness (mm)	1.51	1.57	0.051
Assembly radius (mm)	51		
Temperature change ΔT $(°C)$	100		

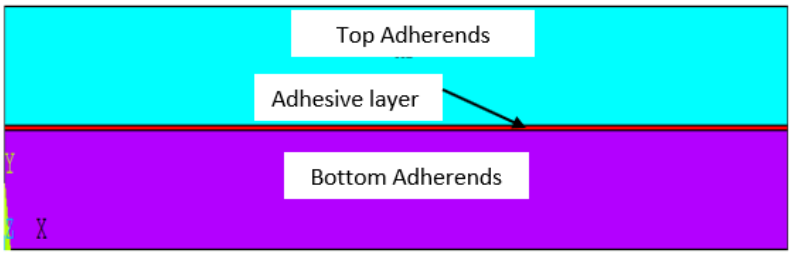

Figure 4.2 Half axisymmetric model of the bonded circular bimaterial thermostat for FEA.

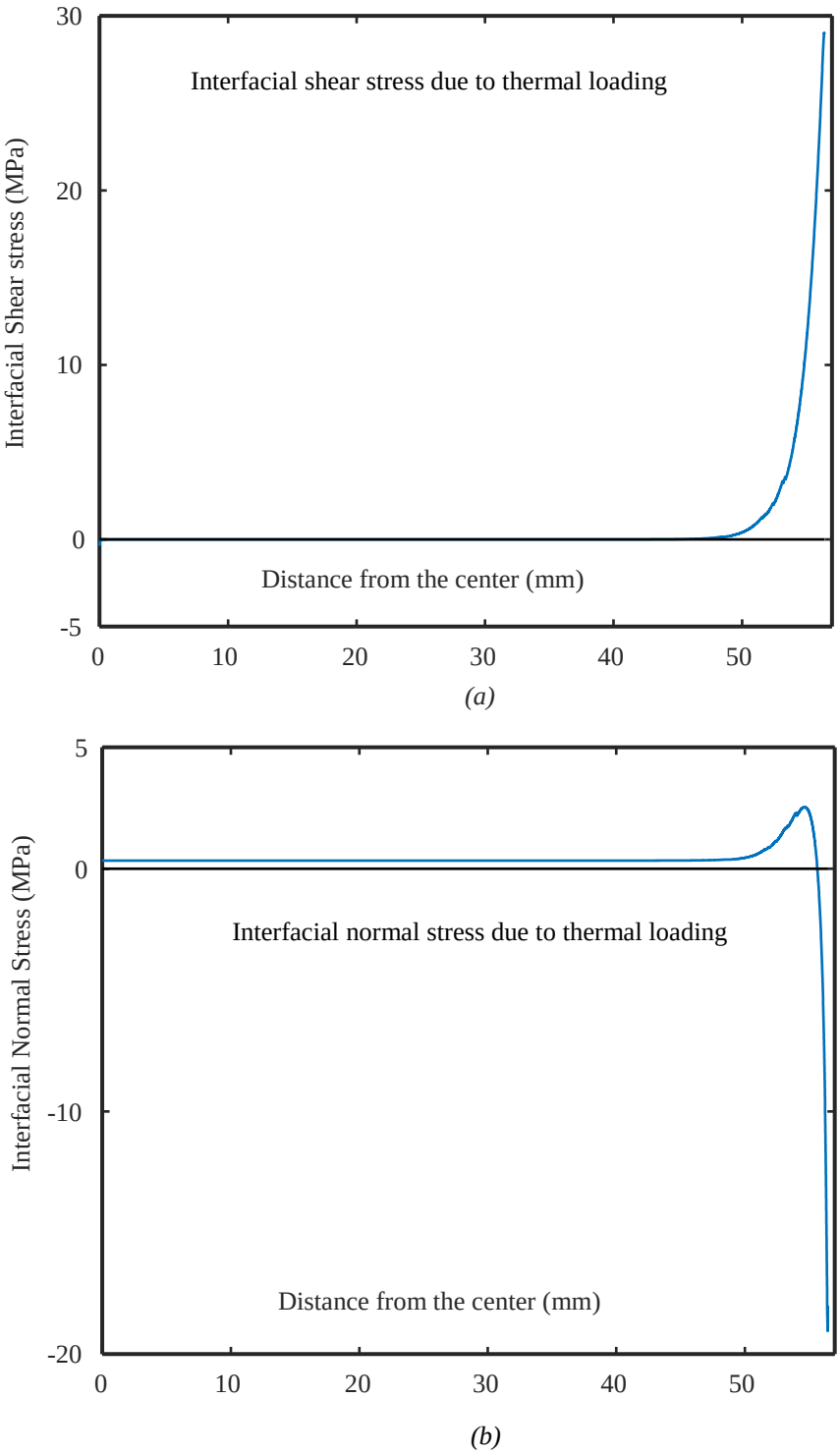

Figure 4.3 FEM-based prediction of the interfacial shear and normal stresses at the interface between two bonded dissimilar materials. (a) Interfacial shear stress and (b) Interfacial normal stress.

4.2.1. Effect of loading and boundary conditions

This section is to discuss the stress analysis with various loading conditions, BCs, and adhesive layer thicknesses within the bonded circular materials. Figure 4.4 shows the interfacial shear and normal stresses of the circular joints, resulted from varying temperature change. The material properties given in Table 4.1 are employed for the FEM-based computational simulation, with the joint radius of 20 mm. The maximum shear stress of 26.6 MPa is determined by FEA with temperature change of $\Delta T = 100℃$, which is higher than that obtained at temperature change of $\Delta T=50℃$. Refined examination of the FEA results shows that the interfacial shear stress is negligibly small along most of the binding line and yet increases significantly only near the free edges. Similarly, a lower temperature change ($\Delta T = 50℃$) corresponds to a lower peak interfacial normal stress of 9.21 MPa, compared to the peak interfacial normal stress of 18.4 MPa at a higher temperature change ($\Delta T = 100℃$). In addition, the normal stress diminishes to zero along the interface, which switches from positive (tensile) to negative (compressive) near the free edges, while the shear stress remains the same direction.

Figure 4.5 shows the variation of interfacial stresses with the varying thickness of the adhesive layer. During the computational process, the same BCs are maintained for the adhesive layer, and, a uniform temperature change of $\Delta T = 100℃$ is applied. In the case study, two distinct thicknesses of the adhesive layer, 0.05 mm and 0.1 mm, are examined, resulting in a maximum shear stress of 28.1 MPa for the thinner layer and 21 MPa for the thicker one. Evidently, the thicker layer suppresses the interfacial shear stress in the bonded circular joint subjected to steady thermal loading. Similarly, the peak interfacial normal stress of the thicker layer is 11.5 MPa, in contrast to the peak interfacial normal stress of 18.4 MPa of the thinner layer

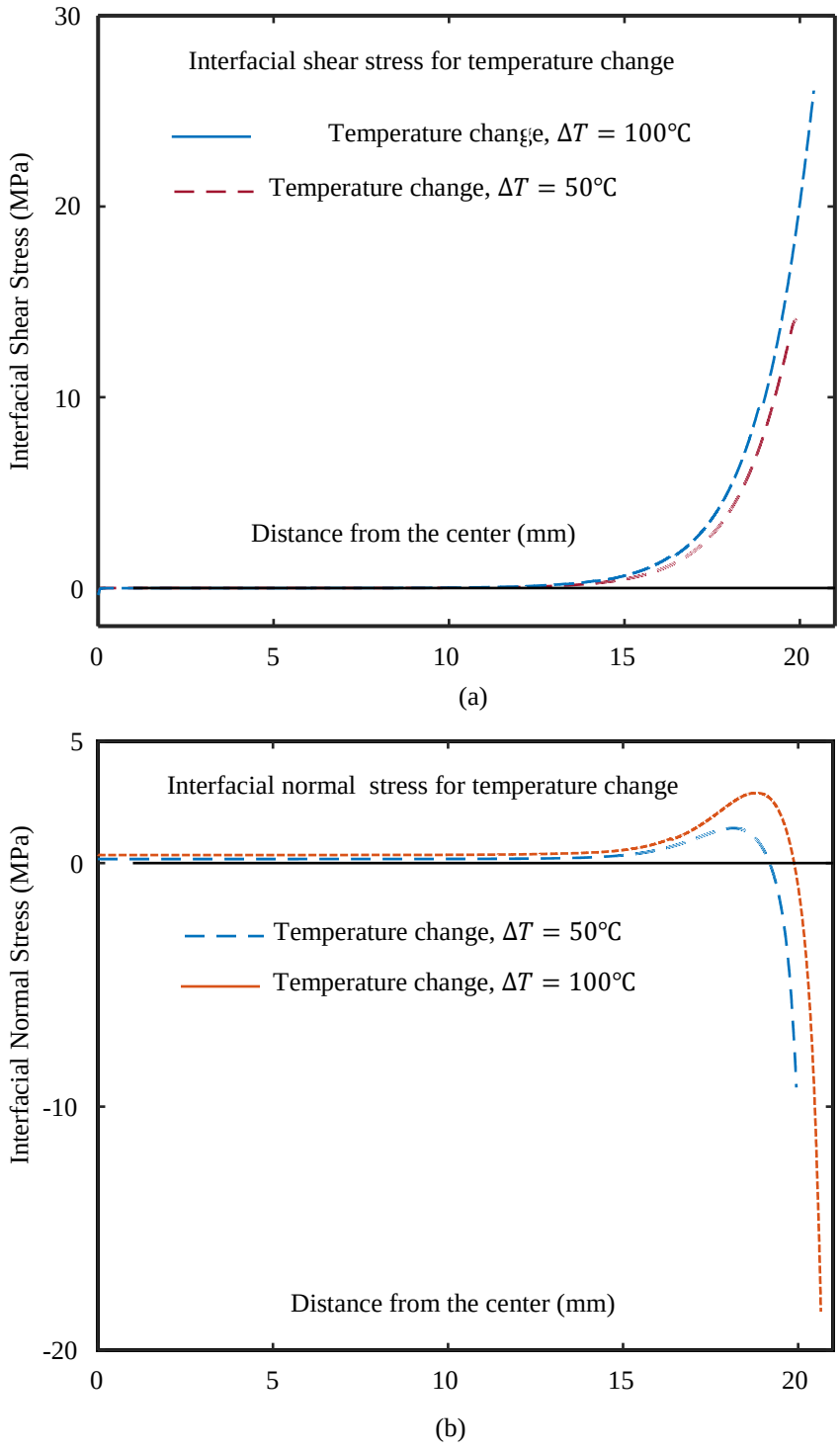

Figure 4.4 FEM-based prediction of the interfacial stresses due to temperature change $\Delta T =$ 50℃ and 100 ℃, respectively. (a) Interfacial shear stress and (b) Interfacial normal stress.

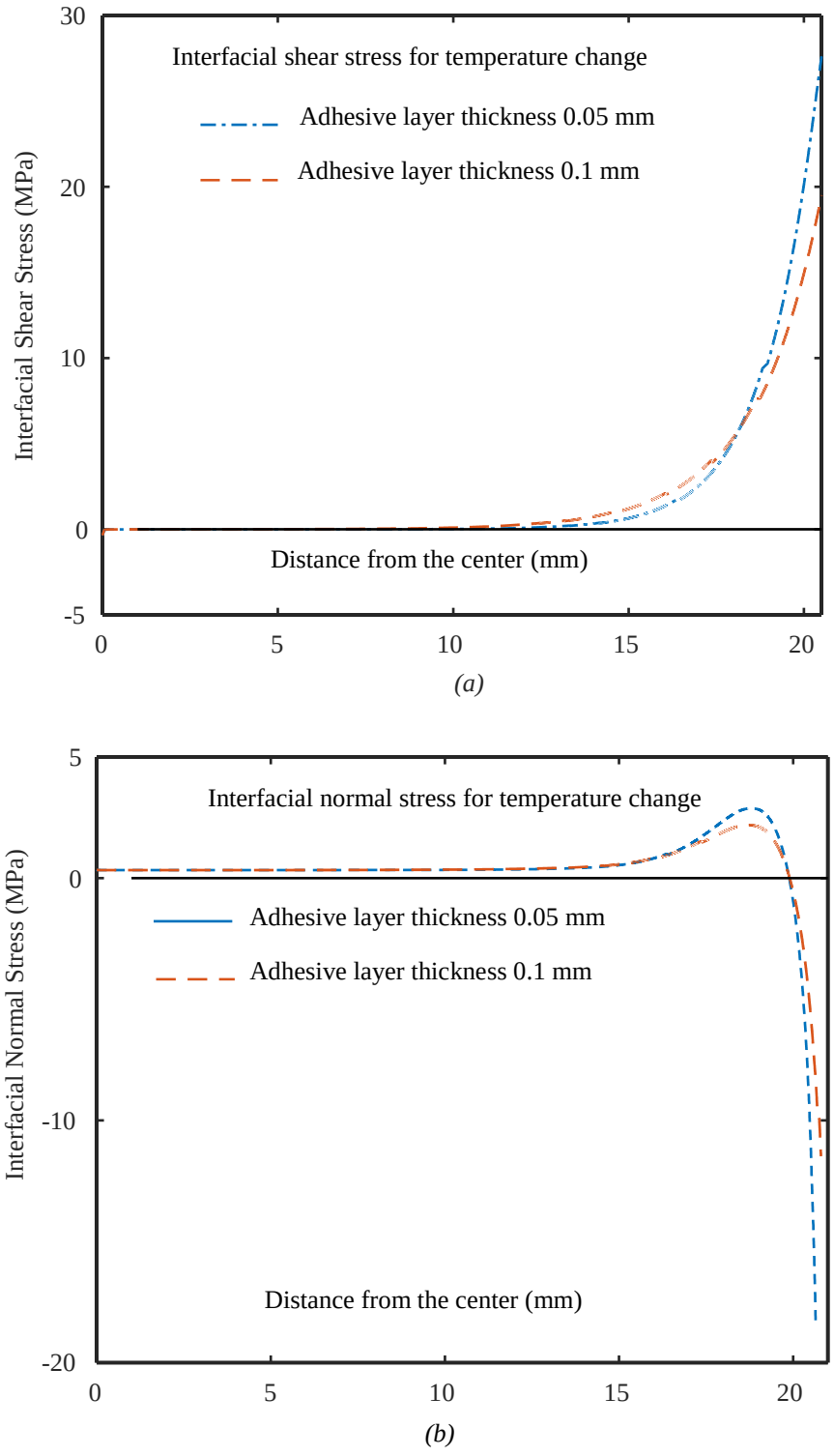

Figure 4.5 FEM-based prediction of the interfacial stresses due to temperature change 100 ℃ at varying thickness of adhesive layer. (a) Interfacial shear stress and (b) Interfacial normal stress.

Figure 4.6 reveals how different BCs affect the interfacial stress of bonded circular joints. Notably, when the bottom adherend is fixed, thereby constraining the free bending, both interfacial shear stress and normal stress exhibit considerable elevation compared to the case that the adherends are free of flexural bending. The use of the non-bending condition results in a maximum shear stress of 45.9 MPa, whereas the presence of bending generates 28.2 MPa, indicating a substantial increase in the interfacial shear stress. Similarly, the interfacial normal stress without bending is measured at 47.2 MPa, while the presence of bending yields 18.2 MPa. It is crucial to emphasize that a thermal load of ΔT=100℃ is applied in this numerical process.

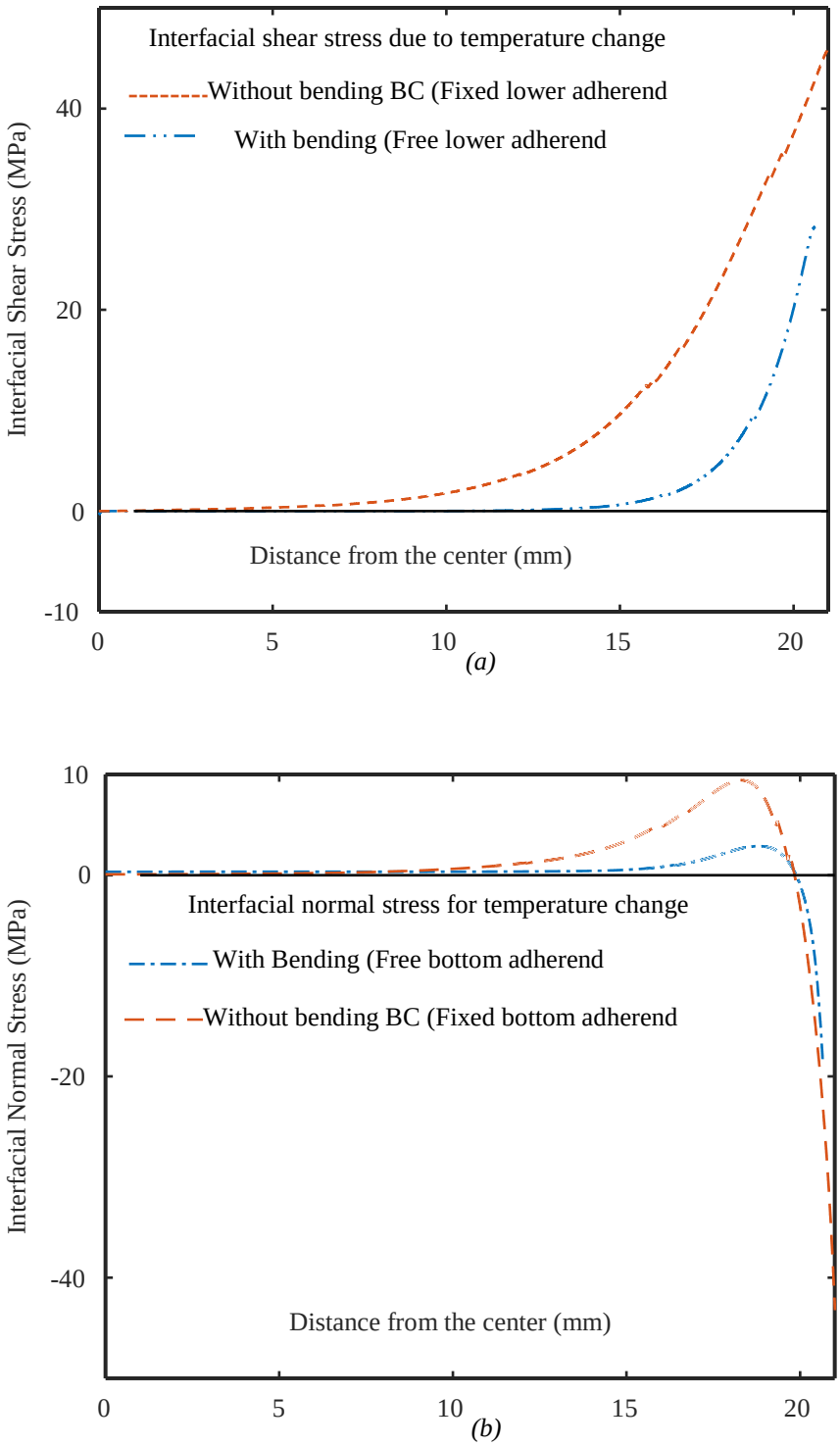

Figure 4.6 FEM-based prediction of the interfacial stresses due to temperature change 100 ℃ at different BCs of bottom layer. (a) Interfacial Shear stress and (b) Interfacial normal stress

4.3. Conclusions

In summary, FEM-based computational modeling is conducted in this chapter to determine the interfacial stresses of bonded circular bimaterial thermostats resulting from thermal loads as a typical example considered in the literature. The present computational study offers valuable insights and resources to understand the stress concentration at free-edges due to mismatch of the elastic properties and coefficients of thermal expansion of two bonded circular materials. The peak shear stress appears at the free edges of joint, which is responsible the debonding of the two bonded materials. As a rule of thumb, FEA is needed to evaluate the structural strength for design optimization and to ensure the superior performance of electronic devices without premature failures.

5. CONCLUSIONS

In summary, PMCs made of compliant polymeric resins (e.g., epoxies) reinforced with high-performance microfibers (e.g., carbon, glass, or plant fibers) have found broad structural applications in aerospace, aeronautical and ground vehicles, marine ships, industrial and civil infrastructures, and sports utilities. Due to their heterogeneous microstructures and large difference of the mechanical properties of resins and reinforcing fibers, the failure of a PMC is typically a progressive cracking process of microcrack nucleation, crack growth, and final catastrophic failure. To ensure the structural reliability and health of PMCs, it is important to develop robust methods for understanding and predicting the failure process and mechanisms of PMCs subjected to external loads and temperature change.

The objective of this study was to develop a semi-analytic stress-function variational method that can accurately and efficiently predict the interfacial stresses and progressive cracking in PMC laminates under external loading. During the process, a classic three-layered symmetric cross-ply PMC laminate with periodic transverse ply cracks is considered. To accurately determine the stress field in the PMC system, two unknown interfacial shear and normal stress functions are introduced at each laminate interface (i.e., ply surface), and the planar stresses of each ply of the laminate are expressed exactly in terms of the stress functions of the upper and lower ply surfaces according to the static equilibrium equations. A set of governing ODEs of the interfacial stress functions are obtained via evoking the principle of minimum complementary strain energy and then solved explicitly in terms of eigenfunctions. The present method ensures the stress field of the cracked PMC laminate to satisfy all the traction BCs at interfaces and crack surfaces. It is needed to mention that for nearly all existing models in the literature, the interfacial shear stresses on the ply surfaces do not satisfy the simple traction-free

condition at crack tips and free edges, and the interfacial normal stresses perpendicular to the ply direction are just simply ignored, i.e., the defection of the longitudinal plies after cracking in the transverse plies is not considered. As one of the major advantages, the present semi-analytic approach has effectively taken into account those BCs in the modeling process.

The current semi-analytic stress-function variational method has been effectively validated via comprehensive FEA based on a commercially available software package (ANSYS^{TM}). Comparative studies demonstrate that this present stress-function variational method is a robust, accurate, and efficient semi-analytical approach for stress analysis of the cross-ply composite laminates under consideration. Contrast to those FEM-based and other analytic methods available in the literature, the present semi-analytic method has showed that it is capable of accurately predicting the interfacial stresses and crack spacing in the PMC laminates. Furthermore, scaling analysis of dependencies of the interfacial stresses and crack spacing in the PMC laminates upon the laminate geometries and elastic properties can be conveniently made. The findings from the present study suggest that a thicker and stiffer mid-ply is susceptible to cracking compared to a thinner and more flexible mid-ply. Consequently, the current model offers valuable insights for laminate design optimization and quantitative comparison of different laminate layup as well as thickness effect.

Addition research efforts can be made to further enhance the current semi-analytic method such as

- Generalizing it for a comprehensive analysis of interfacial stresses and progressive cracking in angle-ply polymer matrix composite (PMC) laminates.

- Extend the applicability of the semi-analytic method to encompass multi-layered coating systems and layered smart material systems, thereby establishing a more versatile analytical framework.
- Expand the method to consider dynamic interfacial stresses in layered materials under both steady (vibrational) and impulsive loadings, contributing to a better understanding of structural responses in diverse composite configurations.
- Develop a semi-analytic stress-function variational method tailored for 3D free-edge interfacial stresses, specifically engineered to facilitate nonlinear stress analysis of layered materials, including considerations of plastic deformations near free edges.

Through implementing the present semi-analytic method, the objective is to make a valuable contribution to the creation of a comprehensive analytical set of tools for accurate characterization of complex mechanical behavior of advanced composite structures across a variety of loading conditions, configurations, and environmental factors.

REFERENCES

[1] G. D. Shaffer, “An Archaeomagnetic Study of a Wattle and Daub Building Collapse,” J. F. Archaeol., vol. 20, pp. 59-75, 1993.

[2] R. M. Jones, "Mechanics of Composite Materials," CRC press, 1998.

[3] X. F. Wu, “Fracture of Advanced Polymer Composites with Nanofiber Reinforced Interfaces,”. Ph.D. dissertation, University of Nebraska-Lincoln, 2003.

[4] R. B. Pipes and N. J. Pagano, “Composite Laminates Under Uniform Axial Extension,” J. Compsite Mater., vol. 4, pp. 538-548, 1970.

[5] N. J. Pagano, “On the Calculation of Interlaminar Normal Stress in Composite Laminate,” J. Compos. Mater., vol. 8, no. 1, pp. 65-81, 1974.

[6] D. D. R. Cartié, M. Troulis, and I. K. Partridge, “Delamination of Z-Pinned Carbon Fiber Reinforced Laminates,” Compos. Sci. Technol., vol. 66, no. 6, pp. 855-861, 2006.

[7] L. A. Mignery, C. T. Sun, and T. M. Tan, "The Use of Stitching to Suppress Delamination in Laminated Composites," ASTM International, 1985.

[8] Y. Iwahori, T. Ishikawa, N. Watanabe, A. Ito, Y. Hayashi, and S. Sugimoto, “Experimental Investigation of Interlaminar Mechanical Properties on Carbon Fiber Stitched CFRP Laminates,” Adv. Compos. Mater., vol. 16, no. 2, pp. 95-113, 2007.

[9] W. X. Wang, Y. Takao, T. Matsubara, and H. S. Kim, “Improvement of the Interlaminar Fracture Toughness of Composite Laminates by Whisker Reinforced Interlamination,” Compos. Sci. Technol., vol. 62, no. 6, pp. 767-774, 2002.

[10] C. V. Singh, “Multiscale Modeling of Damage in Multidirectional Composite Laminates," Ph.D. dissertation, Texas A & M University, 2008.

[11] X. F. Wu, Y. A. Dzenis, and K. W. Strabala, “Free-Edge Stresses and Progressive Cracking in Surface Coatings of Circular Torsion Bars,” Int. J. Solids Struct., vol. 45, no. 7-8, pp. 2251-2264, 2008.

[12] X. F. Wu and R. A. Jenson, “Stress-Function Variational Method for Stress Analysis of Bonded Joints Under Mechanical and Thermal Loads,” Int. J. Eng. Sci., vol. 49, no. 3, pp. 279-294, Mar. 2011.

[13] X. F. Wu and Y. Zhao, “Stress-Function Variational Method for Interfacial Stress Analysis of Adhesively Bonded Joints,” Int. J. Solids Struct., vol. 50, no. 25-26, pp. 4305-4319, 2013.

[14] X. F. Wu and R. A. Jenson, “Semianalytic Stress-Function Variational Approach for the Interfacial Stresses in Bonded Joints,” J. Eng. Mech., vol. 140, no. 11, pp. 1-11, 2014.

[15] X. F. Wu, R. A. Jenson, and Y. Zhao, “Stress-Function Variational Approach to the Interfacial Stresses and Progressive Cracking in Surface Coatings,” Mech. Mater., vol. 69, no. 1, pp. 195-203, 2014.

[16] X. F. Wu and U. Chowdhury, “Fracture Toughness of Adhesively Bonded Joints with Large Plastic Deformations,” Eng. Fract. Mech., vol. 190, pp. 16-30, 2018.

[17] K. L. Reifsnider and R. Jamison, “Fracture of Fatigue-Loaded Composite Laminates,” Int. J. Fatigue, vol. 4, no. 4, pp. 187-197, 1982.

[18] S. Abrate, “Matrix Cracking in Laminated Composites: A Review,” Compos. Eng., vol. 1, no. 6, pp. 337-353, 1991.

[19] J. Isometsii and H. Lahtinen, “Criteria for Matrix Failure in Continuous FRP-Composites- A Literature Study. Part 1: Matrix Cracking,” 1996.

[20] K. W. Garrett and J. E. Bailey, “Multiple Transverse Fracture in 90 Cross-Ply Laminates of a Glass Fiber-Reinforced Polyester,” J. Mater. Sci., vol. 12, pp. 157-168, 1977.

[21] A. Parvizi and J. E. Bailey, “On Multiple Transverse Cracking in Glass Fiber Epoxy Cross-Ply Laminates,” J. Mater. Sci., vol. 13, pp. 2131-2136, 1978.

[22] J. A. Nairn, “Matrix Microcracking in Composites,” Polym. Matrix Compos., vol. 2, pp. 403-432, 2000.

[23] R. Talreja, “Transverse Cracking and Stiffness Reduction in Composite Laminates,” J. Compos. Mater., vol. 19, no. 4, pp. 355-375, 1985.

[24] G. J. Dvorak, N. Laws, and M. Hejazi, “Analysis of Progressive Matrix Cracking in Composite Laminates I. Thermoelastic Properties of a Ply with Cracks,” J. Compos. Mater., vol. 19, no. 3, pp. 216-234, 1985.

[25] G. J. Dvorak and N. Laws, “Analysis of Progressive Matrix Cracking in Composite Laminates II. First Ply Failure,” J. Compos. Mater., vol. 21, no. 4, pp. 309-329, 1987.

[26] N. Laws and G. J. Dvorak, “Progressive Transverse Cracking in Composite Laminates,” J. Compos. Mater., vol. 22, no. 10, pp. 900-916, 1988.

[27] S. C. Tan and R. J. Nuismer, “A Theory for Progressive Matrix Cracking in Composite Laminates,” J. Compos. Mater., vol. 23, no. 10, pp. 1029-1047, 1989.

[28] J. W. Lee and I. Daniel, “Progressive Transverse Cracking of Cross-ply Composite Laminates,” J. Compos. Mater., vol. 24, no. 11, pp. 1225-1243, 1990.

[29] J. M. Whitney, “On the ‘Ply Discount Method’ for Determining Effective Thermo-Elastic Constants of Laminates Containing Transverse Cracks,” Compos. Part A Appl. Sci. Manuf., vol. 36, no. 10 SPEC. ISS., pp. 1347-1354, 2005.

[30] Z. Hashin, “Thermal Expansion Coefficients of Cracked Laminates,” Compos. Sci. Technol., vol. 31, no. 4, pp. 247-260, 1988.

[31] Z. Hashin, “Analysis of Cracked Laminates: A Variational Approach,” Mech. Mater., vol. 4, no. 2, pp. 121-136, 1985.

[32] B. Jean-Marie, “Transverse Cracking and Delamination in Cross-Ply Glass-Fiber and Carbon-Fiber Reinforced Plastic Laminates: Static and Fatigue Loading,” Appl. Mech. Rev., vol. 56, no. 1, pp. 111-147, 2003.

[33] L. N. McCartney, “Theory of Stress Transfer in a 0-90-0 Cross-Ply Laminate Containing a Parallel Array of Transverse Cracks,” J. Mech. Phys. Solids, vol. 40, no. 1, pp. 27-68, 1992.

[34] J. W. Lee, D. H. Allen, and C. E. Harris, “Internal State Variable Approach for Predicting Stiffness Reductions in Fibrous Laminated Composites with Matrix Cracks,” J. Compos. Mater., vol. 23, no. 12, pp. 1273-1291, 1989.

[35] M. Romanowicz, “Progressive Failure Analysis of Unidirectional Fiber-Reinforced Polymers with Inhomogeneous Interphase and Randomly Distributed Fibers Under Transverse Tensile Loading,” Compos. Part A Appl. Sci. Manuf., vol. 41, no. 12, pp. 1829-1838, 2010.

[36] T. E. Tay, G. Liu, V. B. C. Tan, X. S. Sun, and D. C. Pham, “Progressive Failure Analysis of Composites,” J. Compos. Mater., vol. 42, no. 18, pp. 1921-1966, 2008.

[37] J. A. Nairn and D. A. Mendels, “On the Use of Planar Shear-Lag Methods for Stress-Transfer Analysis of Multilayered Composites,” Mech. Mater., vol. 33, no. 6, pp. 335-362, 2001.

[38] A. Aveston, J. Cooper, and G. A. Kelly, “Single and Multiple Fracture,” Conference Proceedings, National Physical Laboratory: The Properties of Fibre Composites, I.P.C. Sci. and Tecnol. Press, 1971, pp. 15-26.

[39] J. Aveston and A. Kelly, “Theory of Multiple Fracture of Fibrous Composites,” J. Mater. Sci., vol. 8, no. 3, pp. 352-362, 1973.

[40] S. G. Lim and C. S. Hong, “Prediction of Transverse Cracking and Stiffness Reduction in Cross-Ply Laminated Composites,” J. Compos. Mater., vol. 23, no. 7, pp. 695-713, 1989.

[41] C. Mittelstedt and W. Becker, “Interlaminar Stress Concentrations in Layered Structures: Part I - A Selective Literature Survey on the Free-Edge Effect Since 1967,” J. Compos. Mater., vol. 38, no. 12, pp. 1037-1062, 2004.

[42] J. N. Reddy, "Energy Principles and Variational Methods in Applied Mechanics (3rd ed.)," John Wiley & Sons, 2017.

[43] S. Timoshenko, and J. N. Goodier, "Theory of Elasticity (2nd ed.)", McGraw-Hill,1951.

[44] H. Hu, "Variational Principles of Theory of Elasticity with Applications (1st ed.)", CRC Press, 1984.

[45] J. W. Hutchinson and Z. Suo, “Mixed Mode Cracking in Layered Materials,” Advances in Applied Mechanics, vol. 29. Elsevier, 1991, pp. 63-191.

[46] T. L. Anderson, "Fracture Mechanics: Fundamentals and Applications (3rd ed.)," CRC Press, 2005.

[47] C. Chen and W.T. Nelson, “Thermal Stress in Bonded Joints,” IBM J. RES. Dev., vol. 23, no. 2, 1979.

[48] E. Suhir, “Predictive Analytical Thermal Stress Modeling in Electronics and Photonics,” Appl. Mech. Rev., vol. 62, no. 4, pp. 1-20, 2009.

[49] E. Suhir, C. Gu, and L. Cao, “Predicted Thermal Stresses in a Circular Assembly with Identical Adherends and with Application to a Holographic Memory Package Design,” J. Appl. Mech. Trans. ASME, vol. 79, no. 1, pp. 1-6, 2012.

[50] J. H. Lau, “A Note on The Calculation of Thermal Stresses in Electronic Packaging by Finite Element Methods,” J. Electron. Packag. Trans. ASME, vol. 111, no. 4, pp. 313-320, 1989.

[51] Z. Hashin, “Finite Thermoelastic Fracture Criterion with Application to Laminate Cracking Analysis,” J. Mech. Phys. Solids, vol. 44, no. 7, pp. 1129-1145, 1996

[52] V. Vinogradov and Z. Hashin, “Probabilistic Energy Based Model for Prediction of Transverse Cracking in Cross-Ply Laminates,” Int. J. Solids Struct., vol. 42, no. 2, pp. 365-392, 2005

[53] A. S. D. Wang and F. W. Crossman, “Initiation and Growth of Transverse Cracks and Edge Delamination in Composite Laminates Part 1. An Energy Method,” J. Compos. Mater., vol. 14, no. 1, pp. 71-87, 1980

[54] K. L. R. Highsmith, A L, “Stiffness Reduction Mechamsms in Composite Laminates,” ASTM STP, vol. 775, p. 103, 1982.

[55] G. J. D. Laws, N., “The Loss of Stiffness of Cracked Laminates,” Proc. IUTAM Eshelby Meml. Symp., p. 119, 1985.